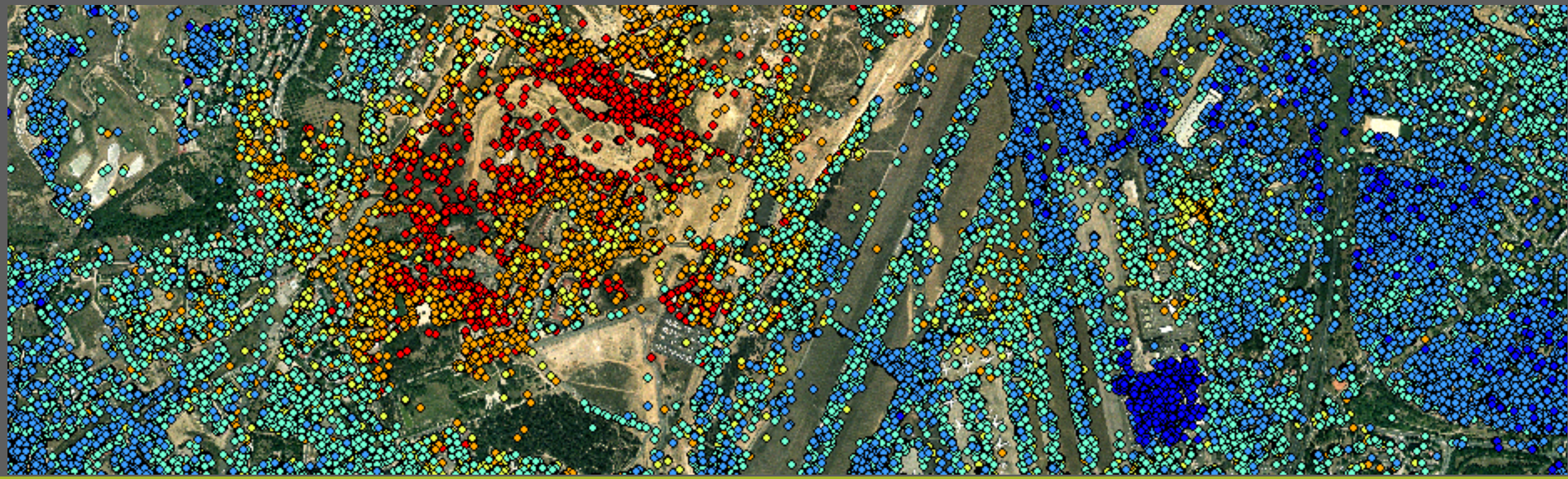

Deteção Remota Microondas

SAR interferometry

João Catalão Fernandes, FCUL


ICEYE

ICEYE builds and operates a commercial constellation of small synthetic aperture radar satellites. So far, 14 satellites have been launched and ICEYE plans to expand its constellation up to 18 satellites by mid-2022, with the objective of reaching an average access time of three hours anywhere on the globe.

The mission is used in many sectors, from monitoring floods and mining activities, to marine vessel detection and iceberg monitoring.

— Rotterdam port from ICEYE

The ICEYE satellite constellation will complement existing synthetic aperture radar missions in the Copernicus programme.

Toni Tolker-Nielsen continued, "We are particularly proud to work with ICEYE, which is one the few New Space companies that we have in Europe in the field of Earth observation. In fact, this is not the first contract that ESA has signed with ICEYE. For a few years now, ESA has been buying ICEYE data and making them available to scientists and to pilot activities. I encourage scientists to use ICEYE data through the Earthnet programme."

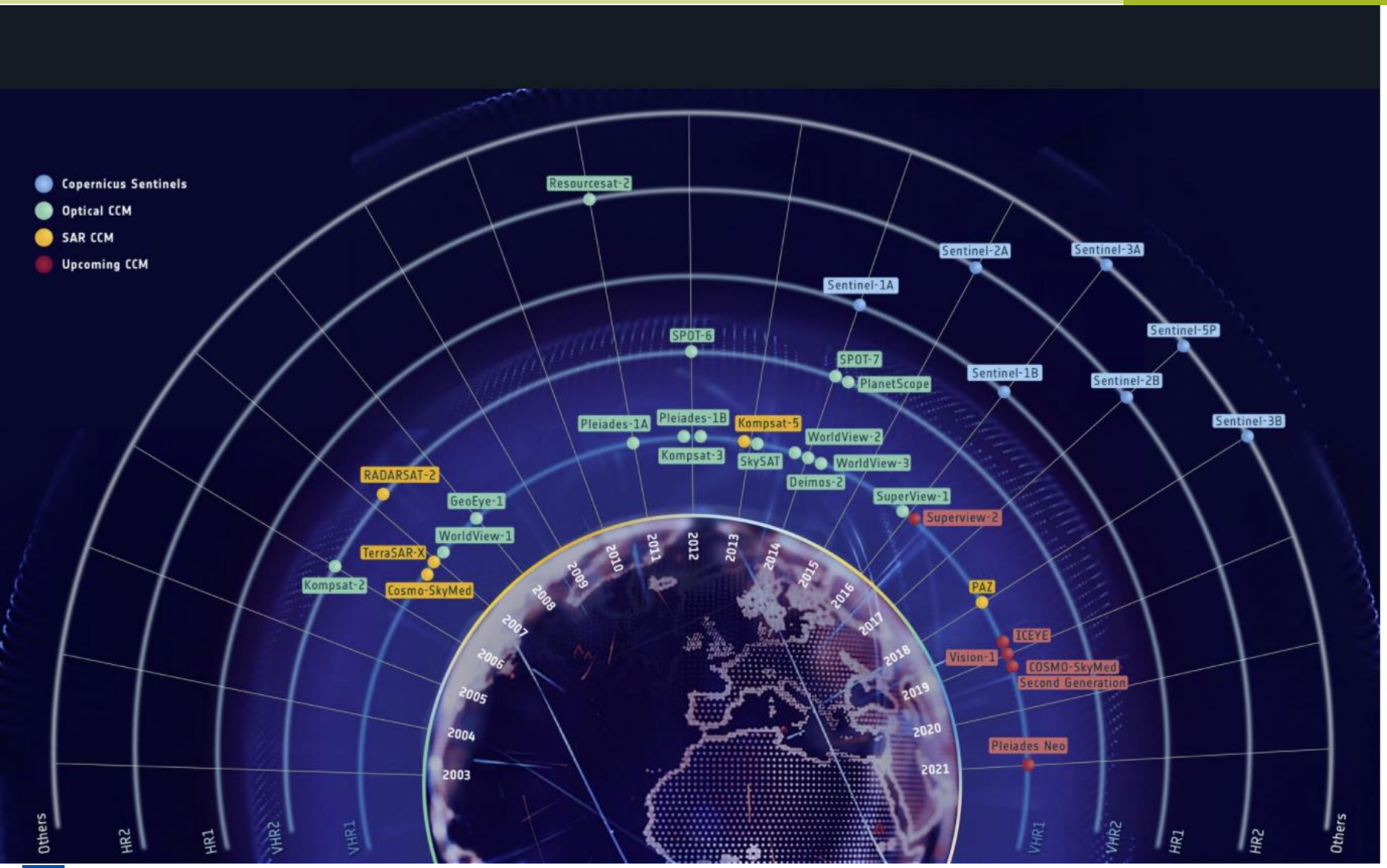

APPLICATIONS

Copernicus Contributing Missions overview

15/09/2021 148 VIEWS 5 LIKES 458918 ID

LIKE DOWNLOAD

Twitter Facebook Copy Link More

DETAILS RELATED

In addition to data provided by the Sentinel satellites, the Copernicus Contributing Missions play a crucial role, delivering complementary data to ensure that a whole range of observational requirements is satisfied. The existing or planned Contributing Missions include missions from ESA, their Member

Topics

- Interferometric Synthetic Aperture Radar (SAR)
- Differential Interferometry
- Atmospheric contribution
- Persistent Scatterer and Time Series Analysis
- PSINSAR Applications
- STAMPS
- InSAR and GPS data fusion
- Mitigating atmospheric effects
- Outlook for SAR interferometry

Geometry from SAR interferometry

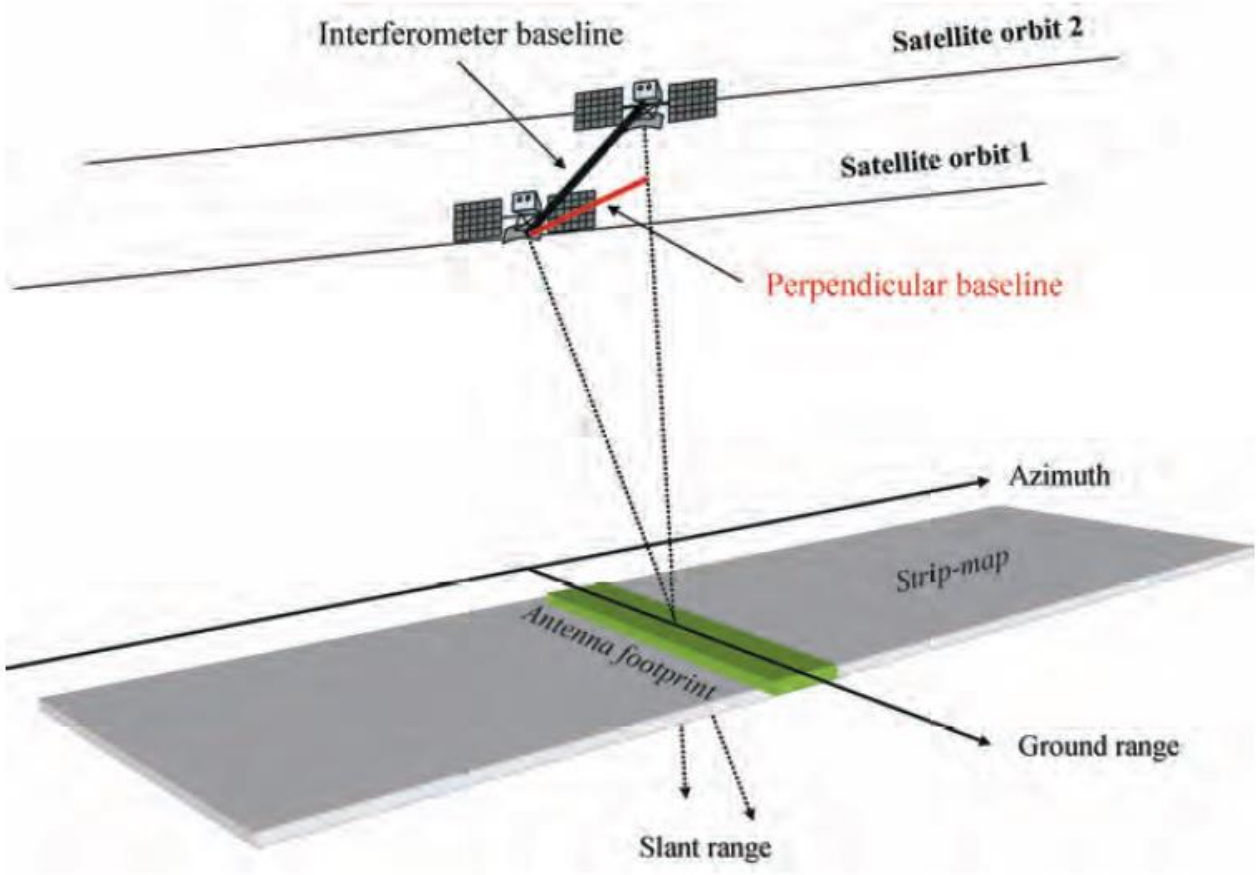

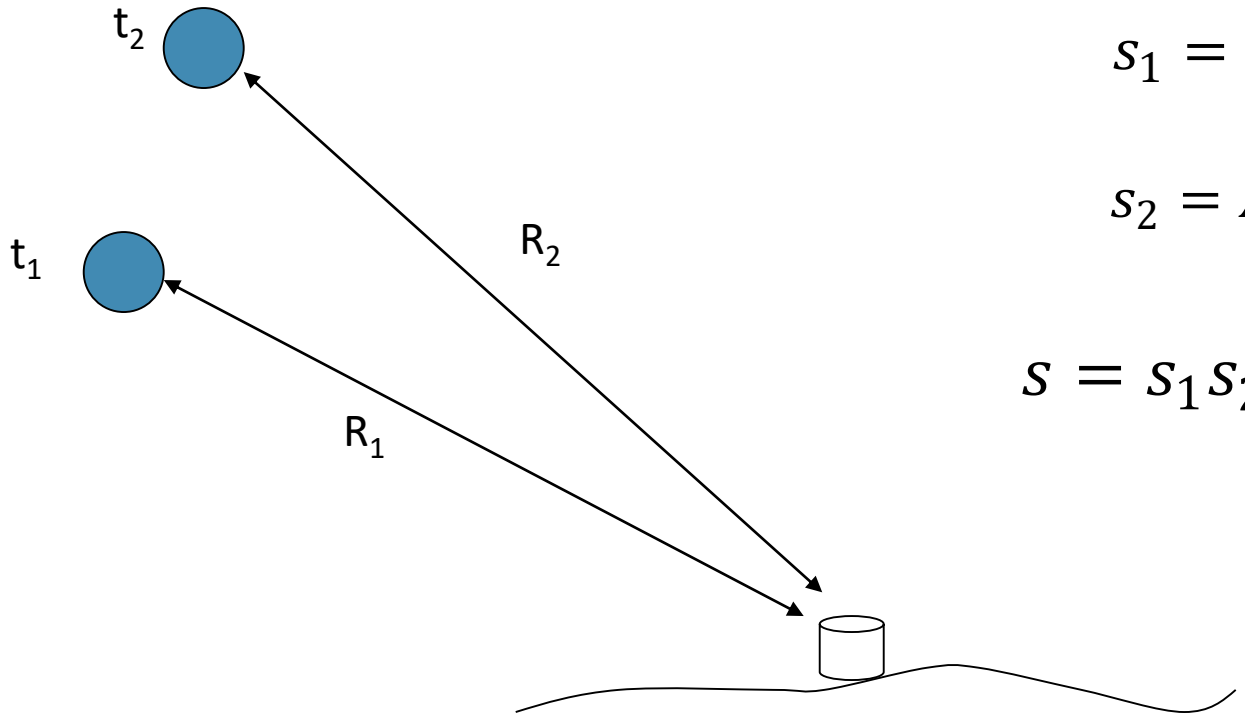

$$s_1 = A.\mathrm{e}^{(j\phi_B)}.e^{\left(-j\left(\frac{4\pi}{\lambda}\right).R_1\right)}$$

$$s_2 = A'.\mathrm{e}^{(j\phi'_B)}.e^{\left(-j\left(\frac{4\pi}{\lambda}\right).R_2\right)}$$

$$s = s_1 s_2^* = |s_1||s_2|\, e^{-j\left(\frac{4\pi}{\lambda}\right).R_1 + j\left(\frac{4\pi}{\lambda}\right).R_2}$$

Interferogram

$$\phi_I = -\frac{4\pi}{\lambda}(R_1 - R_2)$$

If $\phi_B = \phi'_B$, that is, if there is no change in the scattering mechanism of the resolution cell.

First Chapter: Interference

$$E = E_0 (\cos \omega t + i \sin \omega t) = E_0 \exp (i\omega t)$$

$$z = a + ib \qquad E_0 = \sqrt{a^2 + b^2}$$

$$\theta = tan^{-1}\left(\frac{b}{a}\right)$$

$$z = re^{i\theta} = E_1 \cdot E_2^* = |E_0|^2 \cdot e^{i\cdot\left(\frac{2\pi}{\lambda}\cdot[r_2 - r_1] - [\phi_2 - \phi_1]\right)}$$

$$\boxed{\theta = -\frac{4\pi}{\lambda} \cdot [r_1 - r_2]}$$

Interference :: Overview

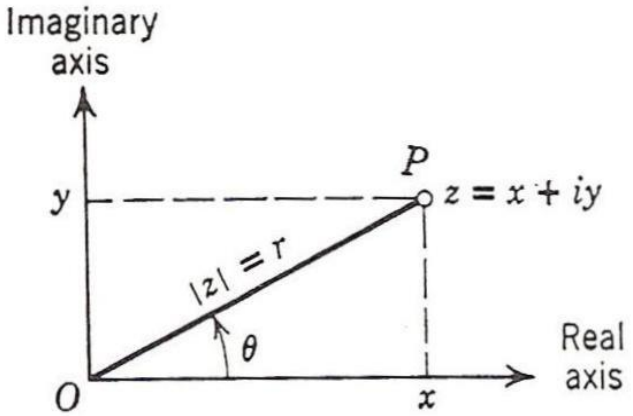

Sem movimento da superfície

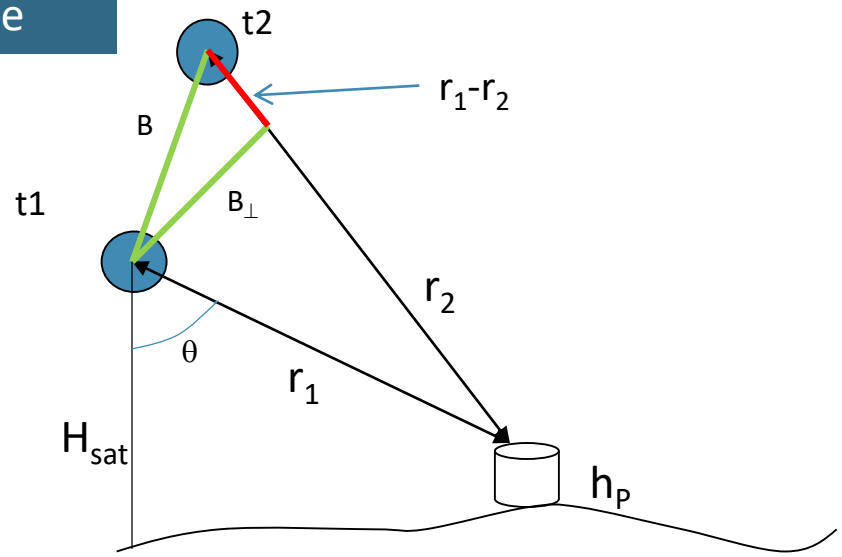

$$h_P = H_{sat} - r_1 \cos\theta$$

$$\phi_{top} = \frac{4\pi}{\lambda}\frac{B_\perp}{r_1 sin\theta} h_p$$

$$Se\ \phi_{top} = 2\pi \Rightarrow h_p = \frac{\lambda r_1 sin\theta}{4\pi B_\perp} 2\pi = \frac{\lambda r_1 sin\theta}{2B_\perp}$$

(Height ambiguity)

$B_\perp$=100m
$h_{2\pi}$= 146 m

With surface movement

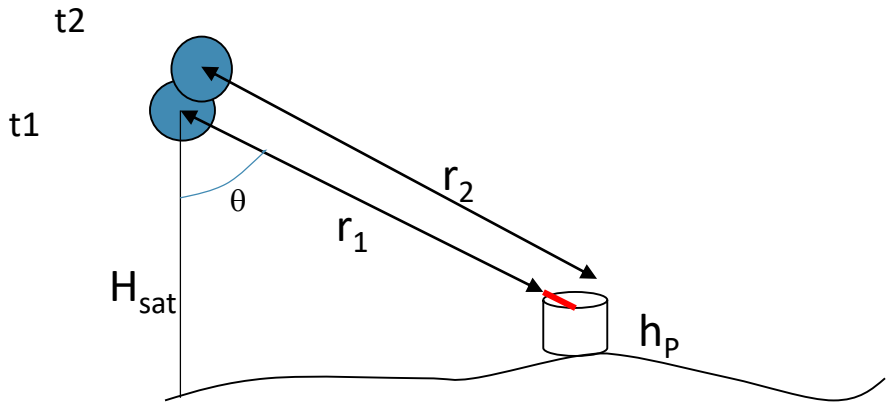

$$\phi_I = \phi_{top} - \frac{4\pi}{\lambda}(r_1 - r_2)$$

$$\phi_I = -\frac{4\pi}{\lambda}\delta r_{desloc} + \frac{4\pi}{\lambda}\frac{B_\perp}{r_P\ sin\theta_P} h_P$$

Sensitivity to deformation 1000x higher than for topography

B = 100m
k=0.003

Fase Topográfica

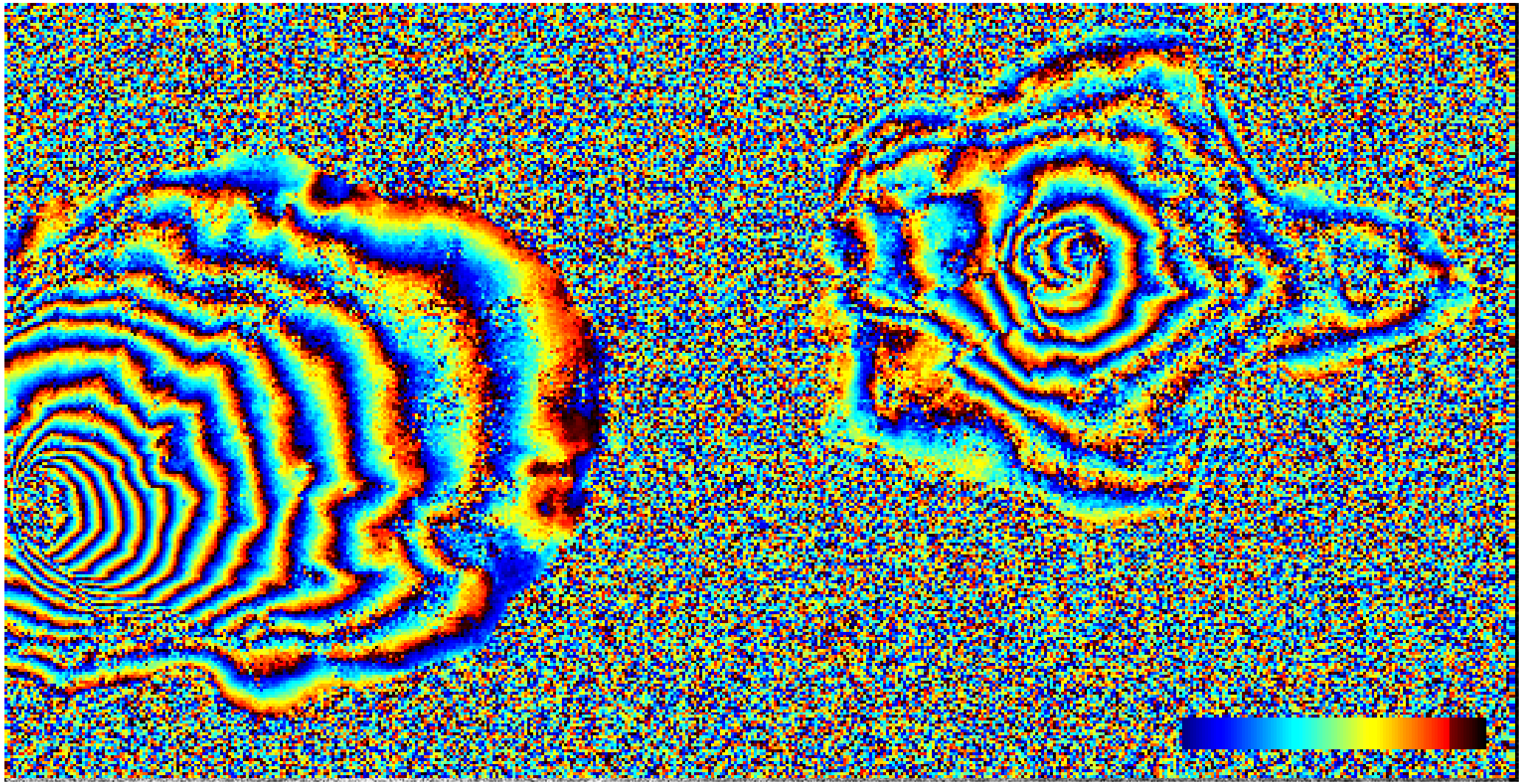

Height ambiguity = 112 m, B = 100m, θ=40º

Differential interferogram

$$\phi_I = -\frac{4\pi}{\lambda}\delta r_{desloc} + \frac{4\pi}{\lambda}\frac{B_\perp}{r_P\ sin\theta_P}h_P \quad \Rightarrow \quad \phi_{Def} = \frac{4\pi}{\lambda}\frac{B_\perp}{r_P\ sin\theta_P}h_P - \phi_I$$

h_P

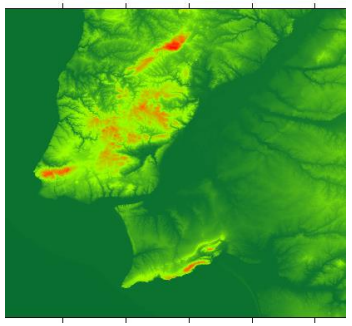

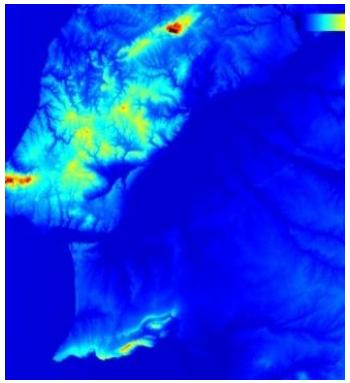

$$\frac{4\pi}{\lambda}\frac{B_\perp}{r_P\ sin\theta_P}h_P$$

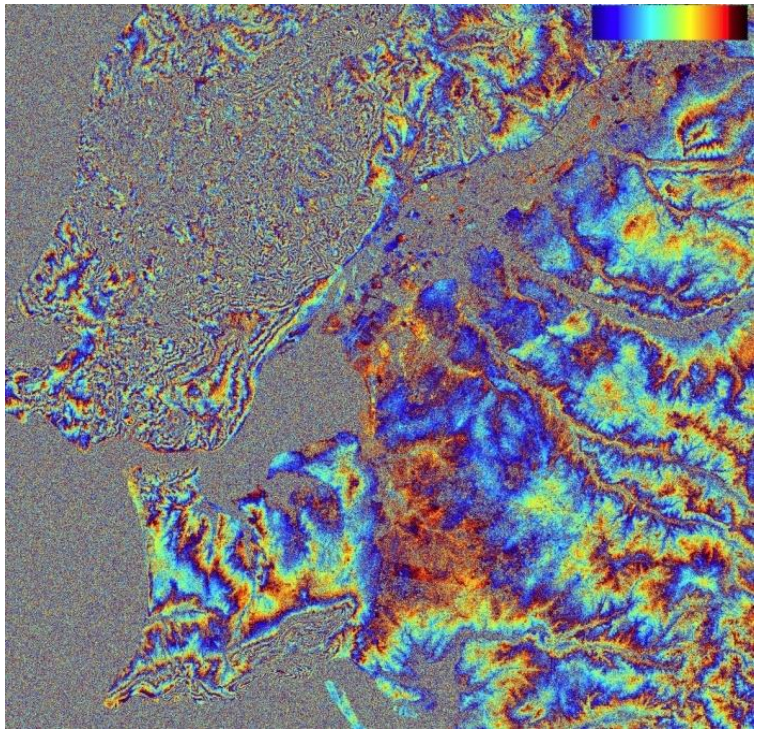

ϕ_I

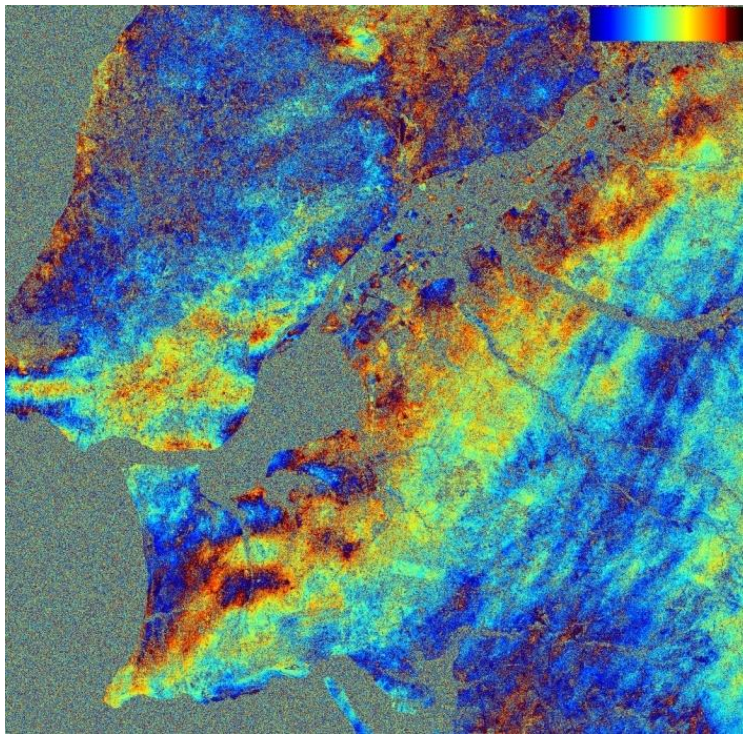

$$\phi_{Def} = \frac{4\pi}{\lambda}\frac{B_\perp}{r_P\ sin\theta_P}h_P - \phi_I$$

João Catalão Fernandes (jcfernandes@fc.ul.pt)

APPLICATIONS

Sentinel-1D preparations underway in

08/10/2025 587 VIEWS 16 LIKES

ESA / Applications / Observing the Earth / Copernicus / Sentin

The Copernicus Sentinel-1 mission is about to get
Sentinel-1D has now undergone the checks and fi
integration with Ariane 6, ready for launch on Tues

Why two satellites are better than one

The launch of Copernicus Sentinel-1D will provide a much-needed replacement to Sentinel-1A, which has been in orbit for 11 years now, well beyond its planned lifetime.

Sentinel-1C has been fully commissioned and currently operates with Sentinel-1A to deliver radar images of Earth's surface, performing in all weathers, day-and-night. This service is vital for disaster response teams, environmental agencies, maritime authorities, climate scientists – and other users who depend on frequent updates of critical data.

Having two satellites in operation at any one time is essential for providing timely data and can mean a significant difference between a late warning and a critical early warning. The arrival of Sentinel-1D will enhance the Sentinel-1 mission's performance in several ways:

When it joins its sibling Sentinel-1C, which was placed in orbit in December 2024, Sentinel-1D will significantly enhance the capabilities of the Copernicus Earth observation programme.

— Sentinel-1D spacecraft with AIS antennas

1. **Better revisit time and coverage:** With two satellites in the same orbit 180° apart, the revisit rate over any location on Earth improves. This means more frequent imaging, faster change detection, better monitoring.

2. **Enhanced features working in synergy:** Both satellites have a C-band Synthetic Aperture Radar (SAR) instrument on board, which allows it to capture high-resolution imagery of Earth's surface. They are also equipped with an Automatic Identification System (AIS) instrument to improve detection and tracking of ships. When both are operational, more frequent AIS observations are possible.

3. **Streamlined operations and cost savings:** Because Sentinel-1C has just gone through commissioning, lessons learned can be applied to Sentinel-1D, reducing time and risk.

4. **GNSS compatibility:** There are other improved onboard capabilities for Sentinel-1. For example, while Sentinel-1A and -1B were compatible only with the Global Positioning System (GPS), Sentinel-1C and -1D are compatible with the whole Global Navigation Satellite System (GNSS), including Galileo.


ThalesAlenia Space
REMOVE BEFORE FLIGHT
STC SENTINEL 1
cnes
inel-1D_container_opens_in_Kourou

Sea-level monitoring satellite unboxed

01/10/2025 2593 VIEWS 18 LIK

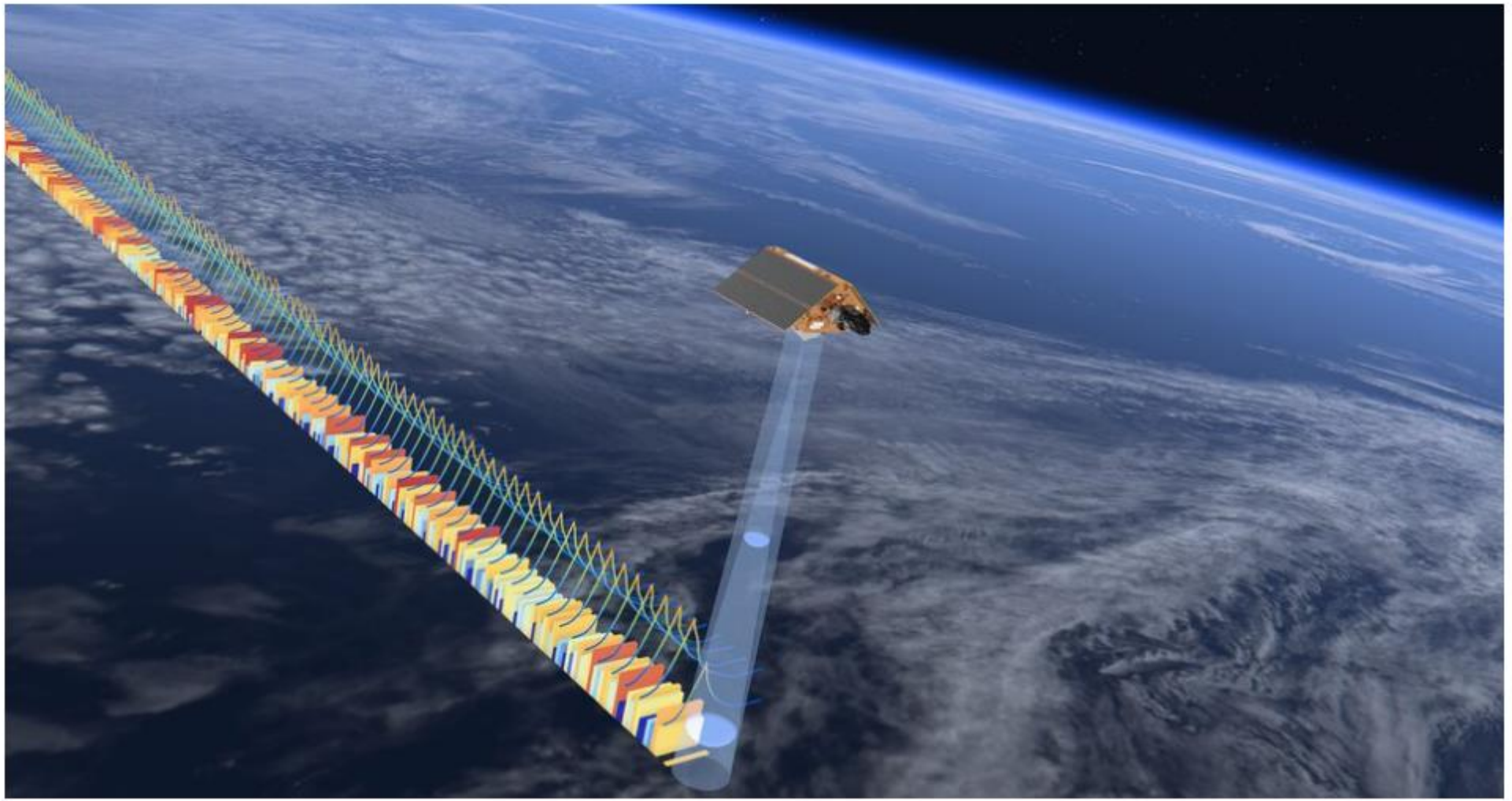

— Copernicus Sentinel-6 radar altimeter

Although part of the European Union's fa

exceptional international cooperation, in

NOAA, with additional support from the

As well as mapping the height of the sea

also provides data for practical 'operatio

wave height and wind speed, data that a

altimetry provides the most comprehens

The Sentinel-6 satellites carry an altimet

travel to Earth's surface and back again

altimetry measurements yield the height

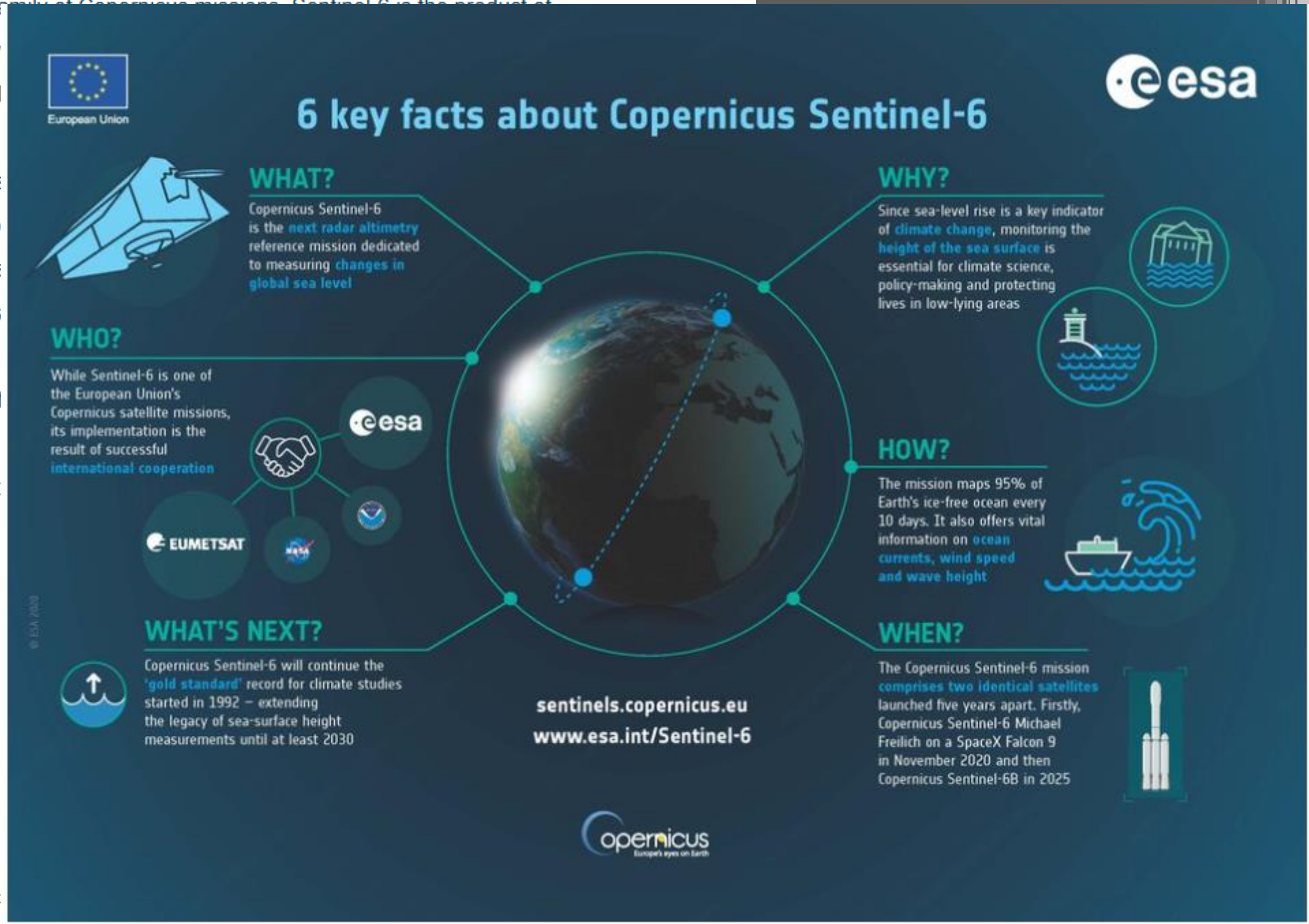

The measure of the phase quality of an interferogram is given by the coherence of each pixel in the interferogram.

Rodriguez and Martin (1992) presented an analytic expression for phase variance:

$$\sigma_\phi^2 = \frac{1}{2N_L}\frac{1-\gamma^2}{\gamma^2}$$

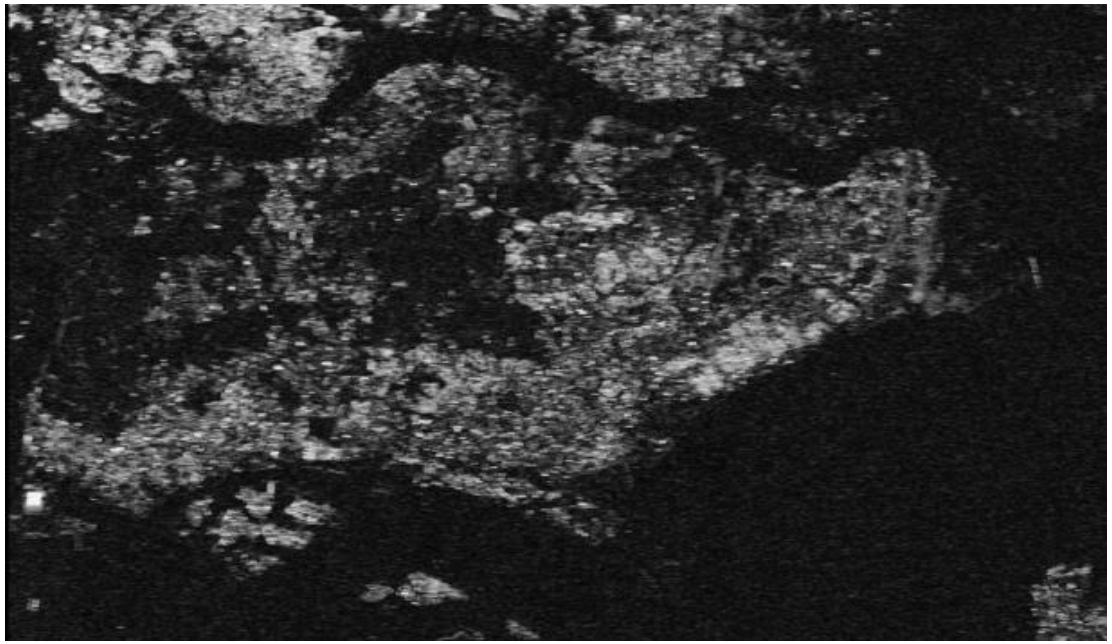

Coherence is defined as:

$$\gamma = \frac{E(s_1 s_2^*)}{\sqrt{E\{|s_1|^2\}.E\{|s_2|^2\}}} \qquad 0 \leq |\gamma| \leq 1$$

DINSAR Applications

- Volcano deformation
- Earthquake deformation
- Permafrost and Glaciar displacement

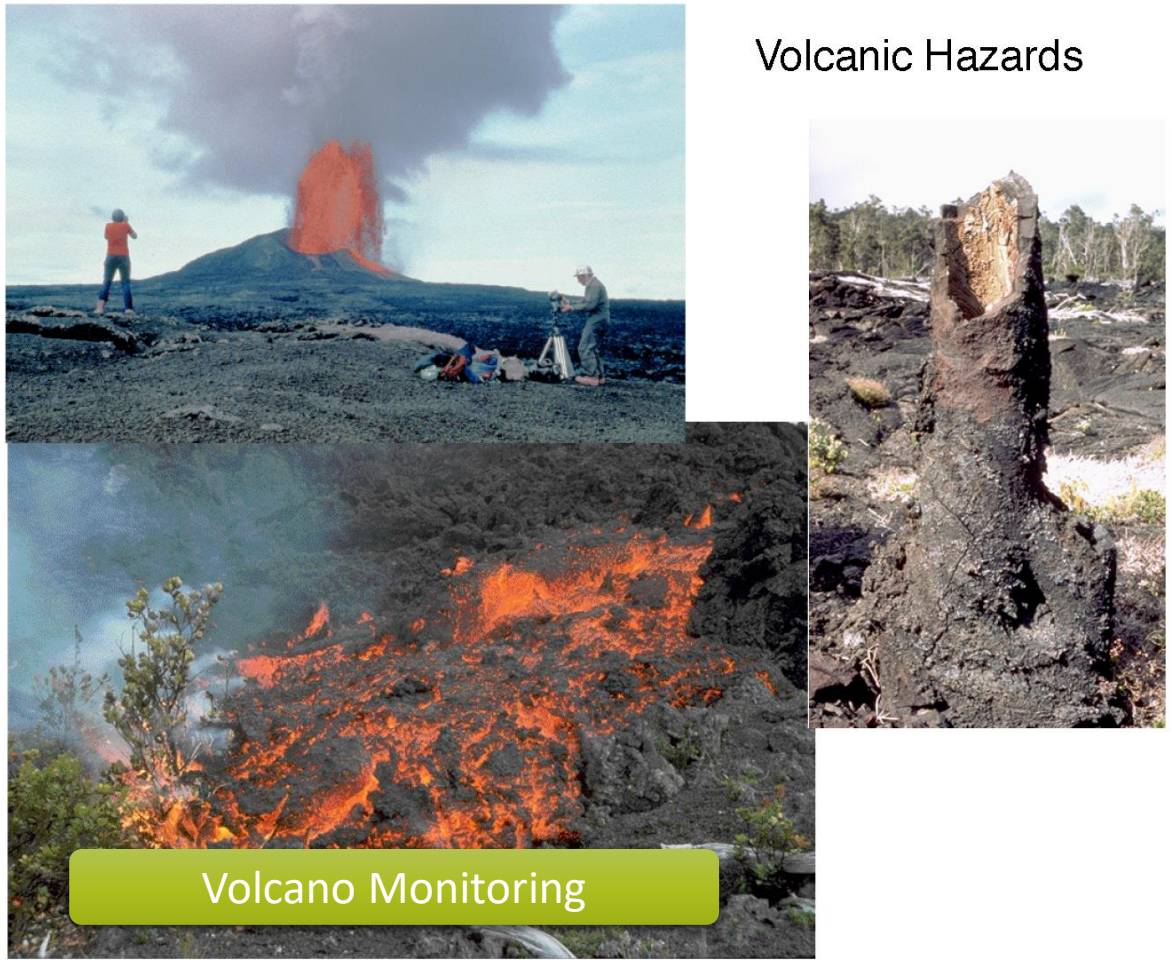

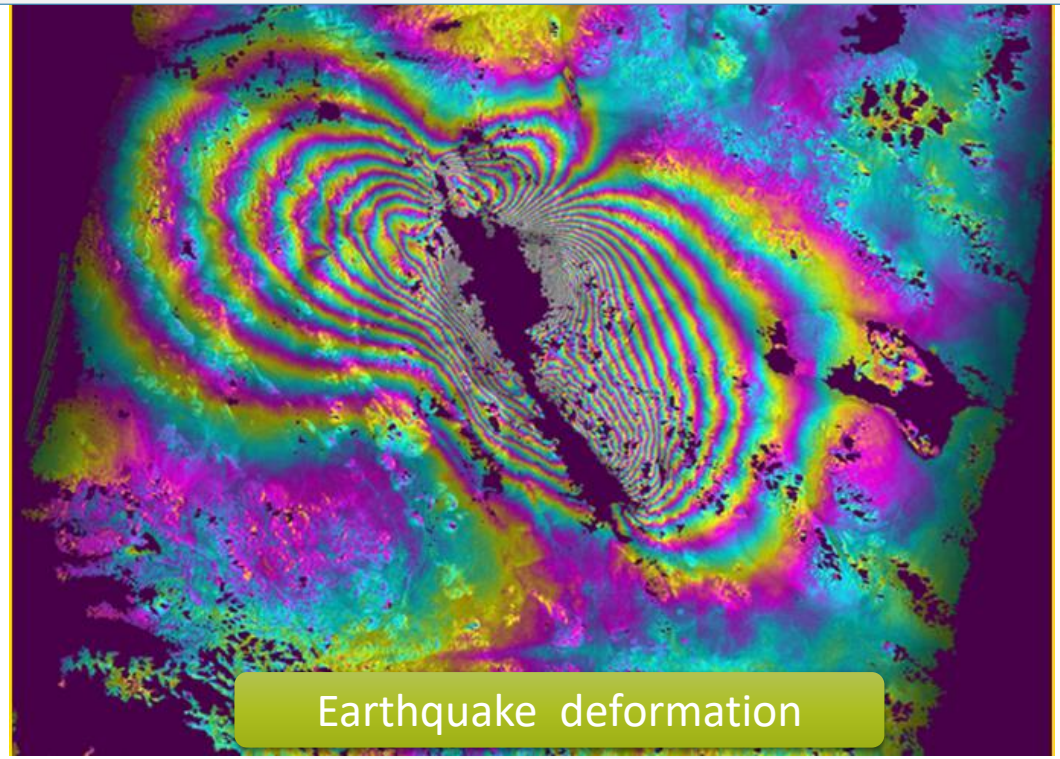

Volcano Monitoring

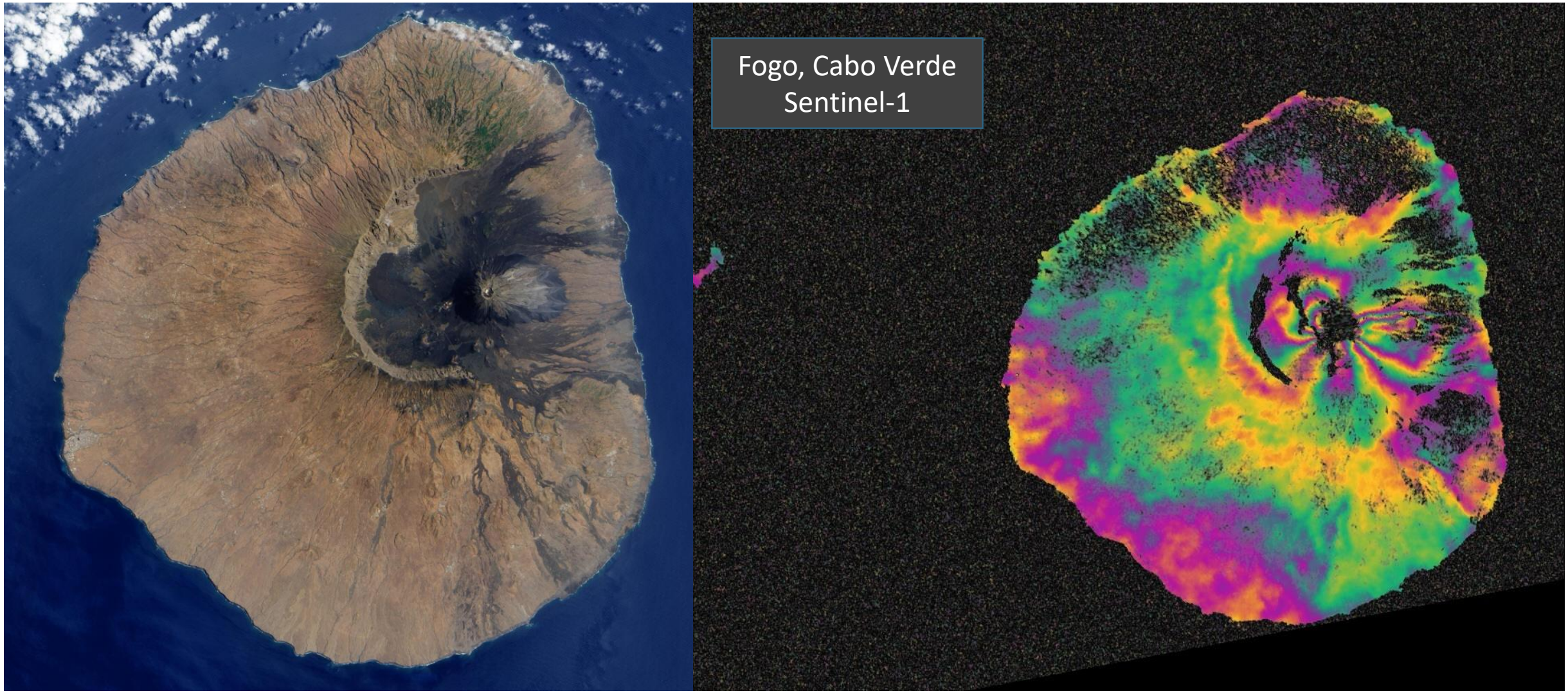

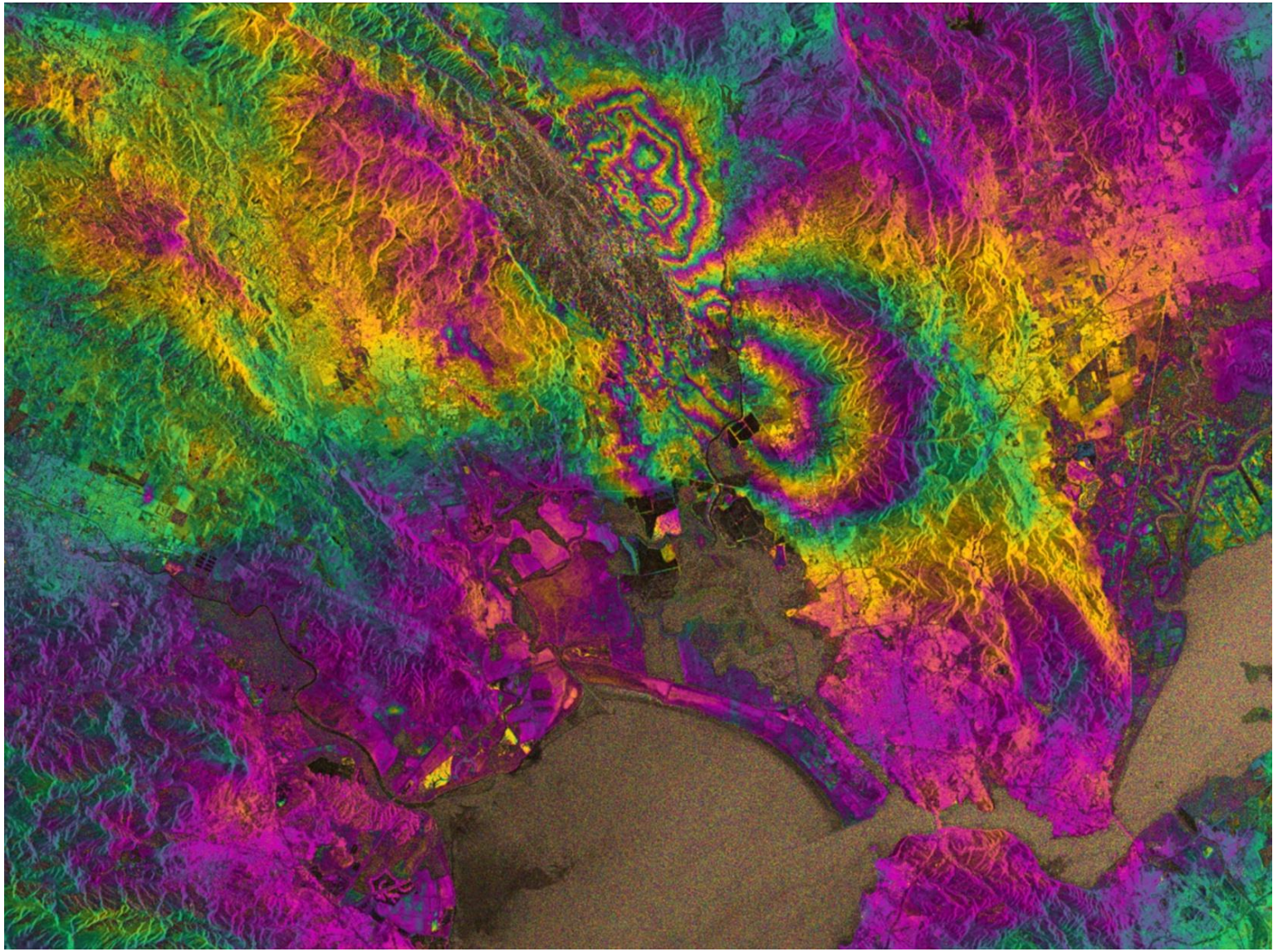

Earthquake deformation

Napa Valey earthquake, 24 Agosto 2014

Sentinel -1

RockGlaciar movement

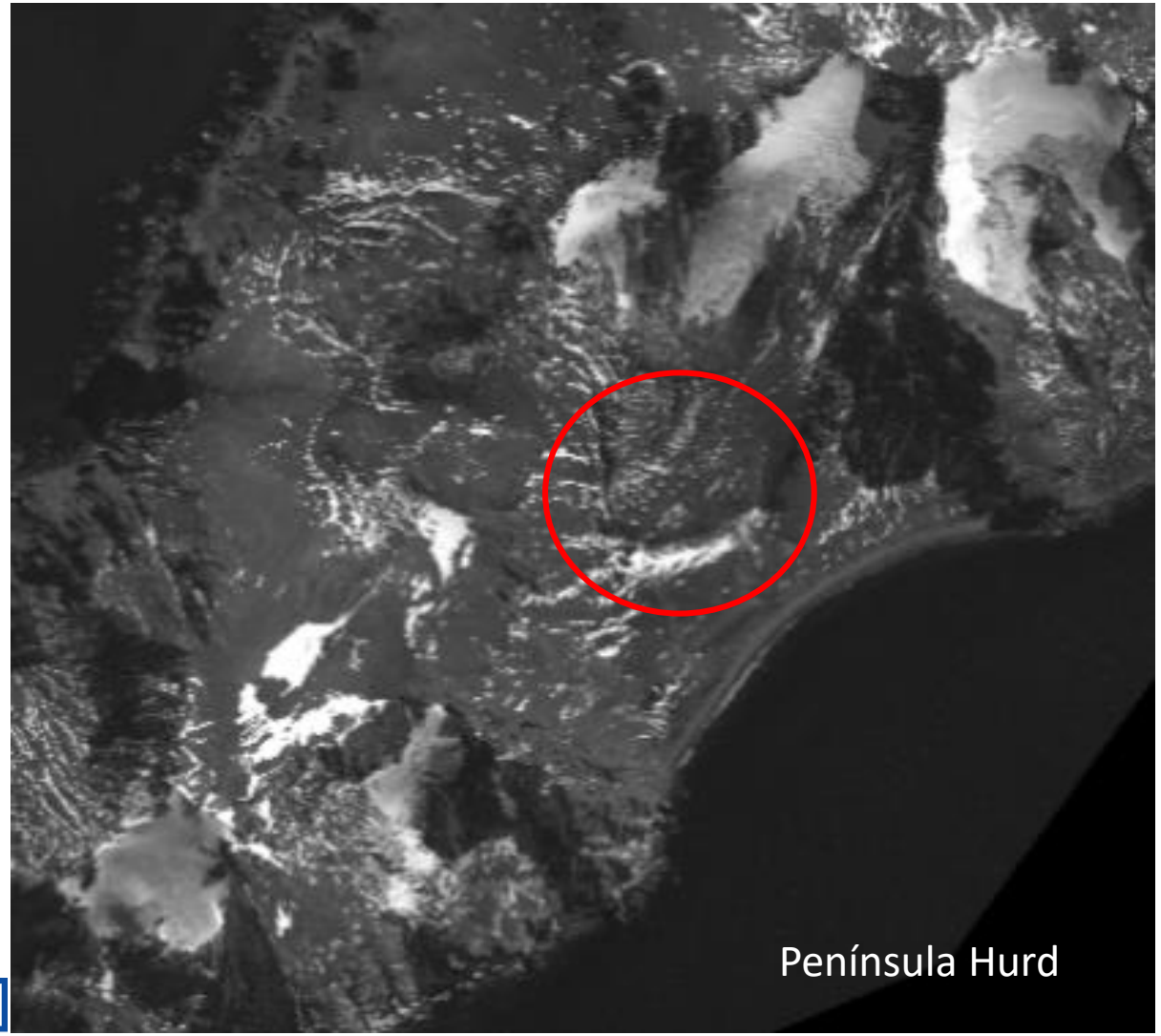

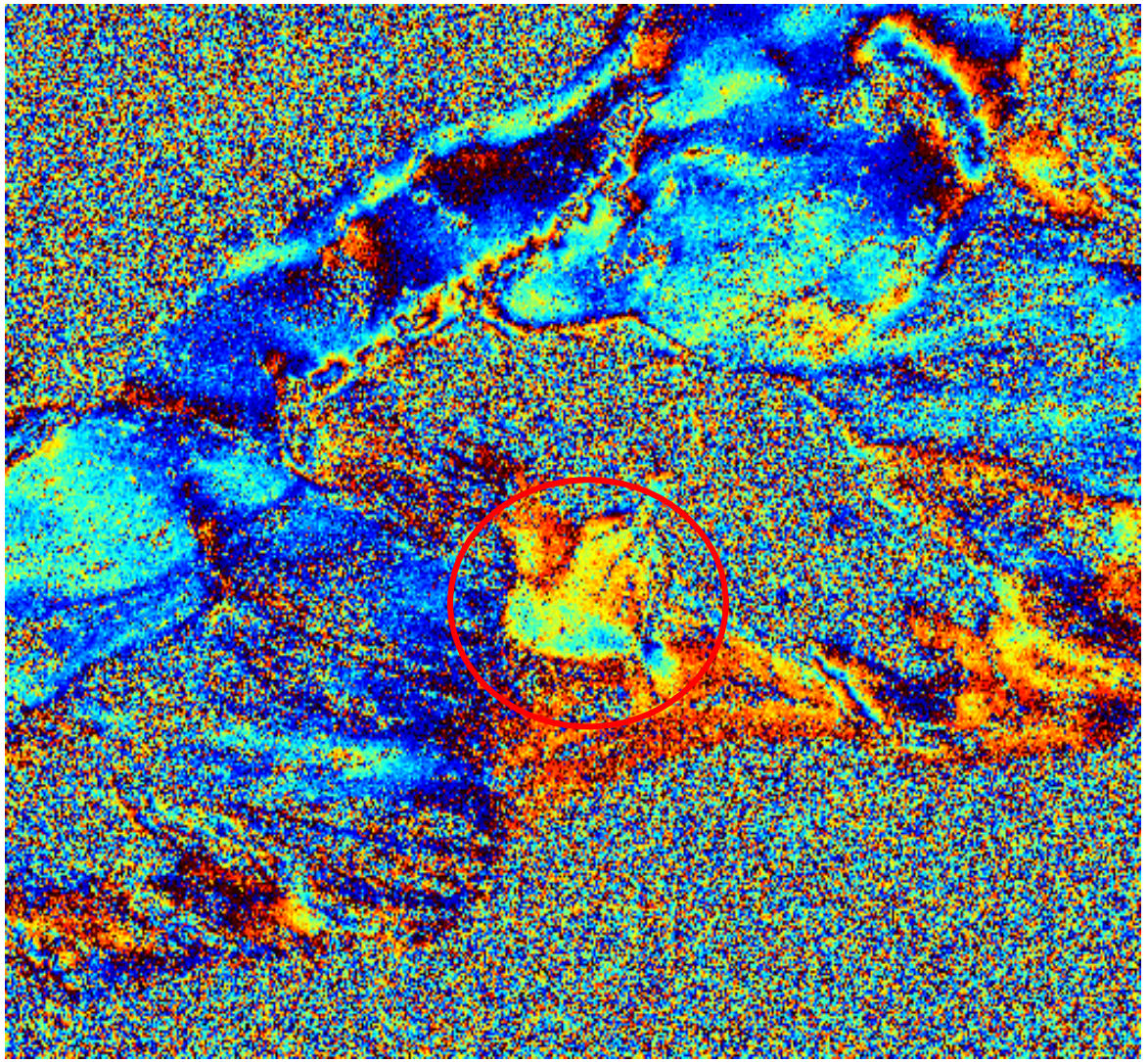

RockGlaciar movement

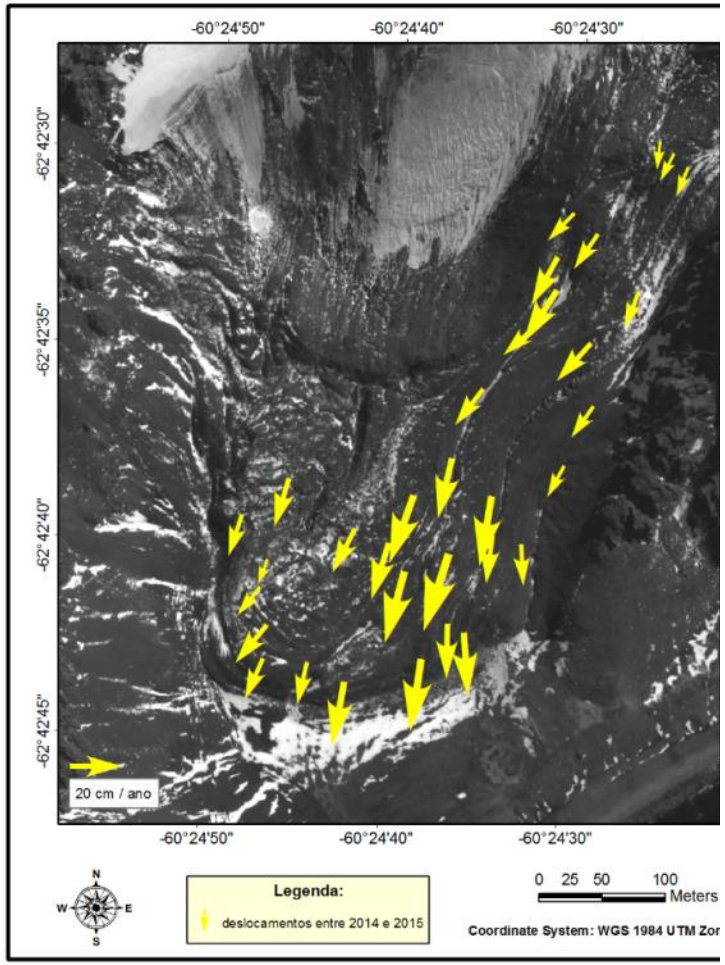

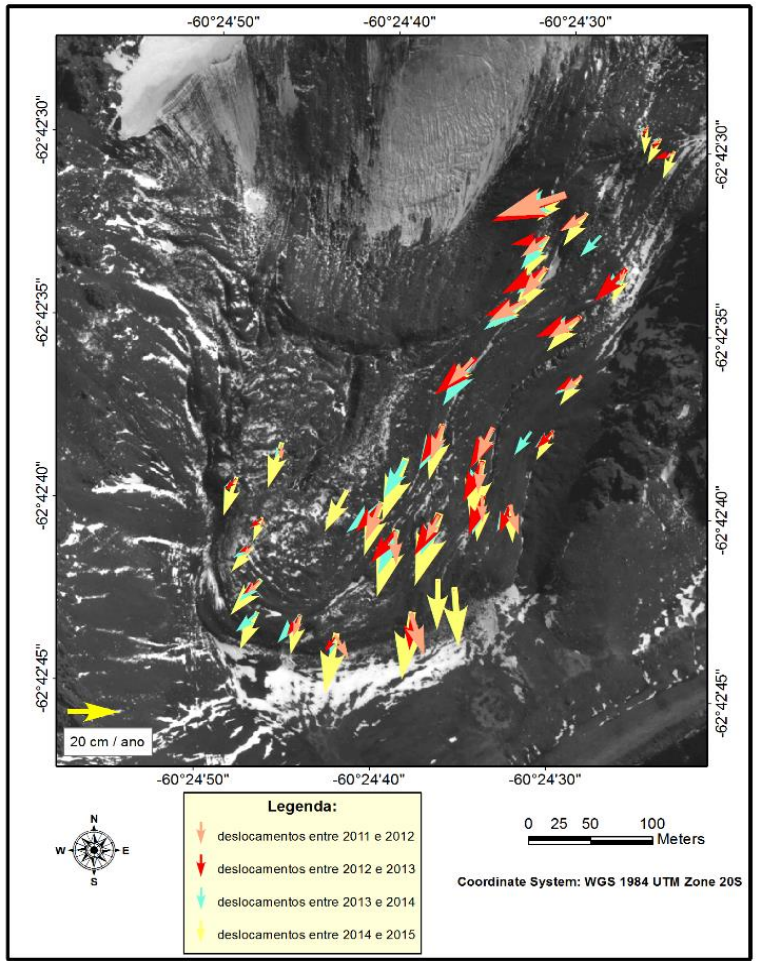

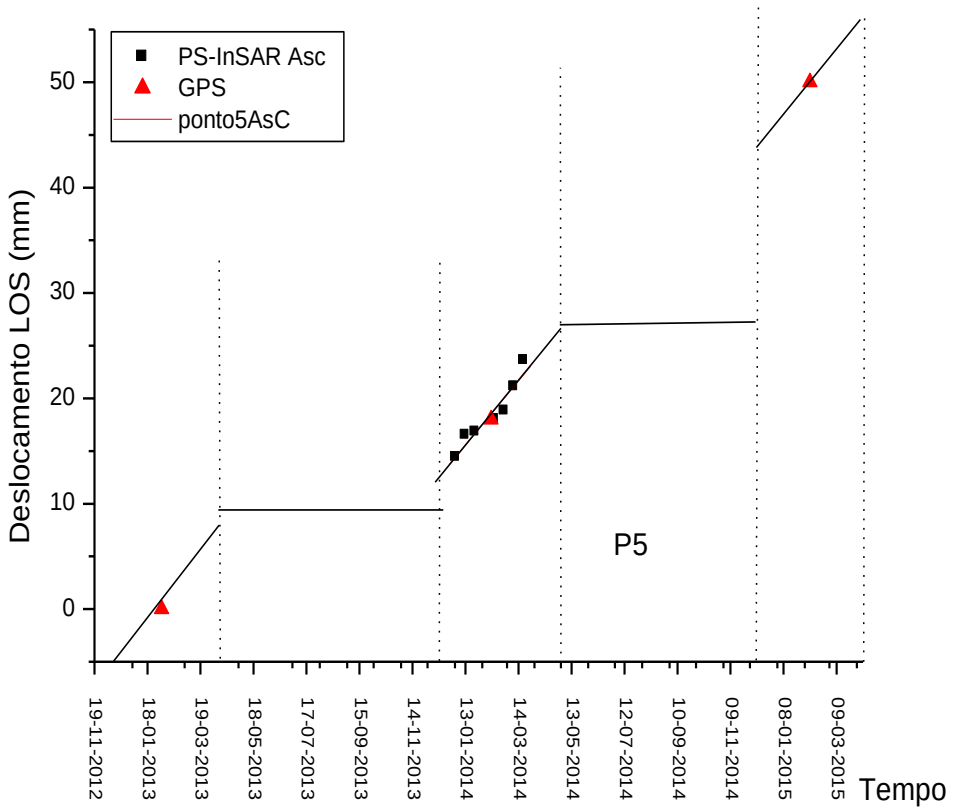

The atmospheric contribution

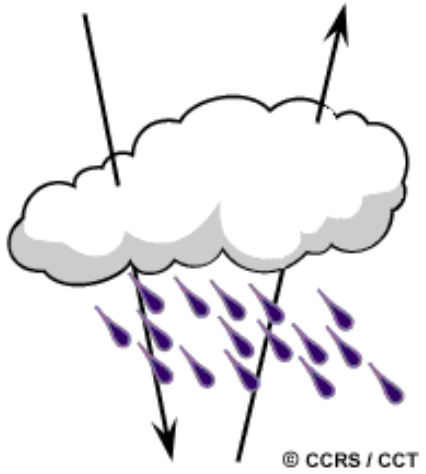

Longer wavelength microwave radiation can penetrate through cloud cover, haze, dust, as the longer wavelengths are not susceptible to atmospheric scattering.

BUT

Radiation travel path can be affected by atmospheric humidity, temperature and pressure

Two SAR images not simultaneous, can be affected differently by the atmosphere with consequences on the interferometric phase.

Limitations of Differential InSAR

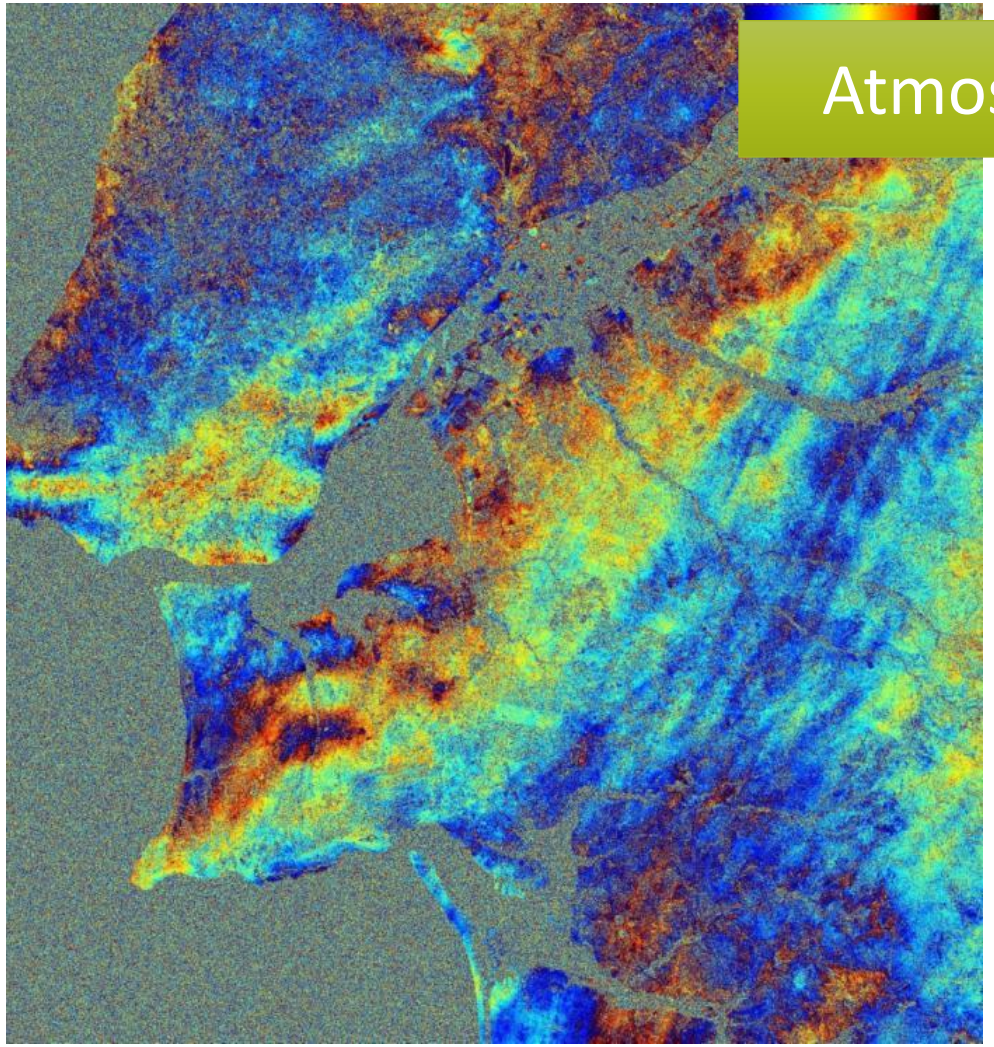

Atmospheric effects

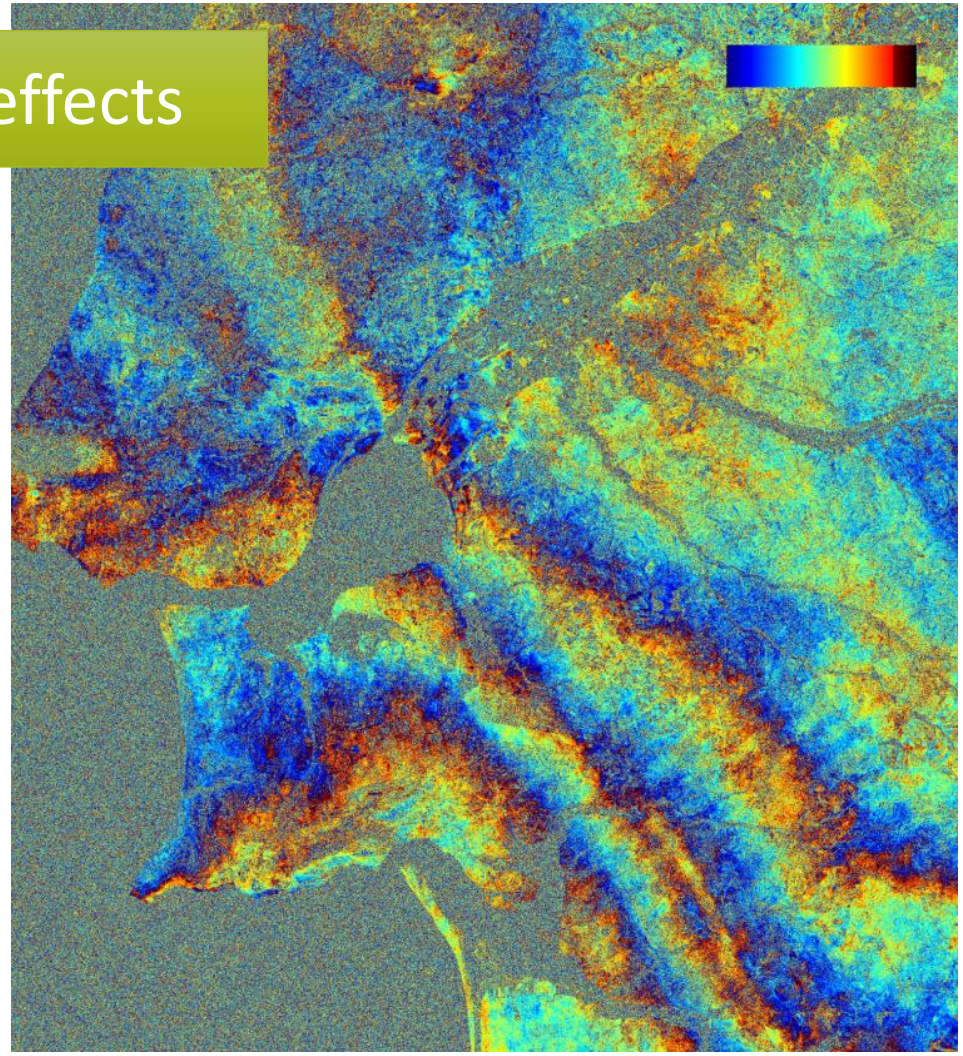

Limitations of Differential InSAR

Geometric decorrelation

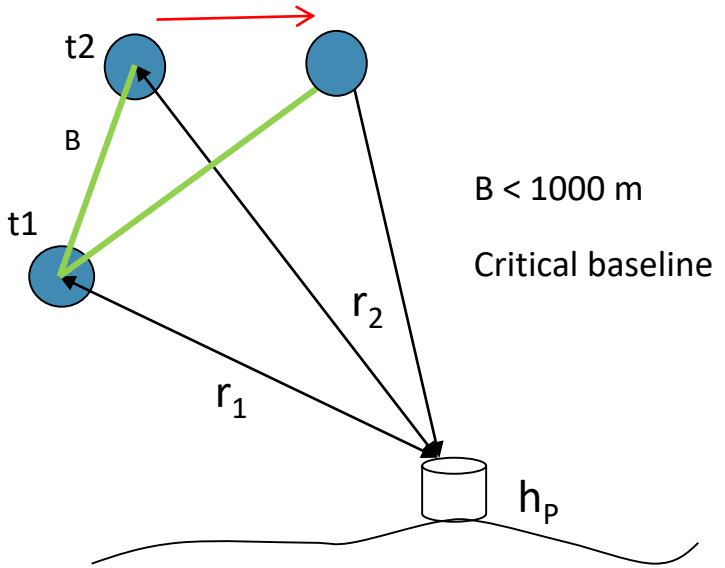

B < 1000 m

Critical baseline

Temporal Decorrelation

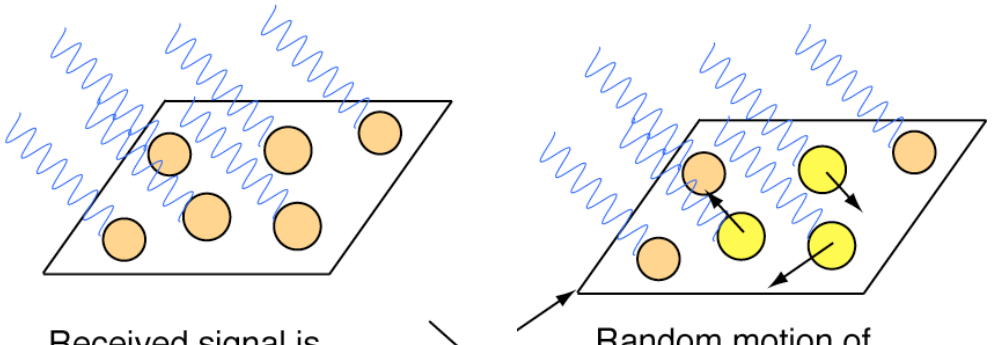

Received signal is superposition of waves from all scattering centers

Random motion of scatterers causes wavelets to interfere- "temporal decorrelation"

$$s_2 = A.\mathrm{e}^{(\phi'_B)}.e^{\left(-j\left(\frac{4\pi}{\lambda}\right).r_2\right)}$$

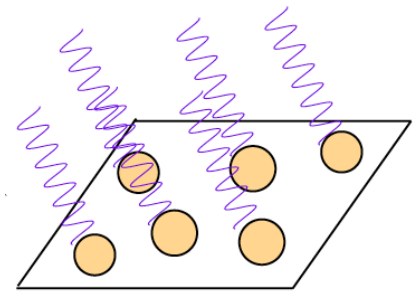

Change in incidence angle causes wavelets to interfere- "baseline decorrelation"

Coherence

What distinguishes this pixel from others?

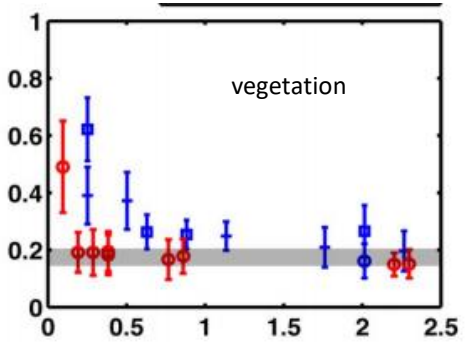

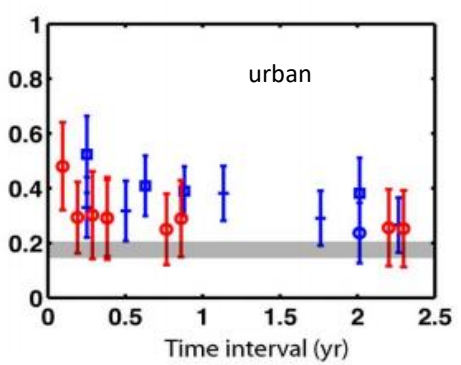

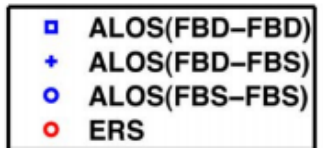

Wei and Sandwell, 2010 (IEEE TGRS)

Persistent Scatterer (PS)

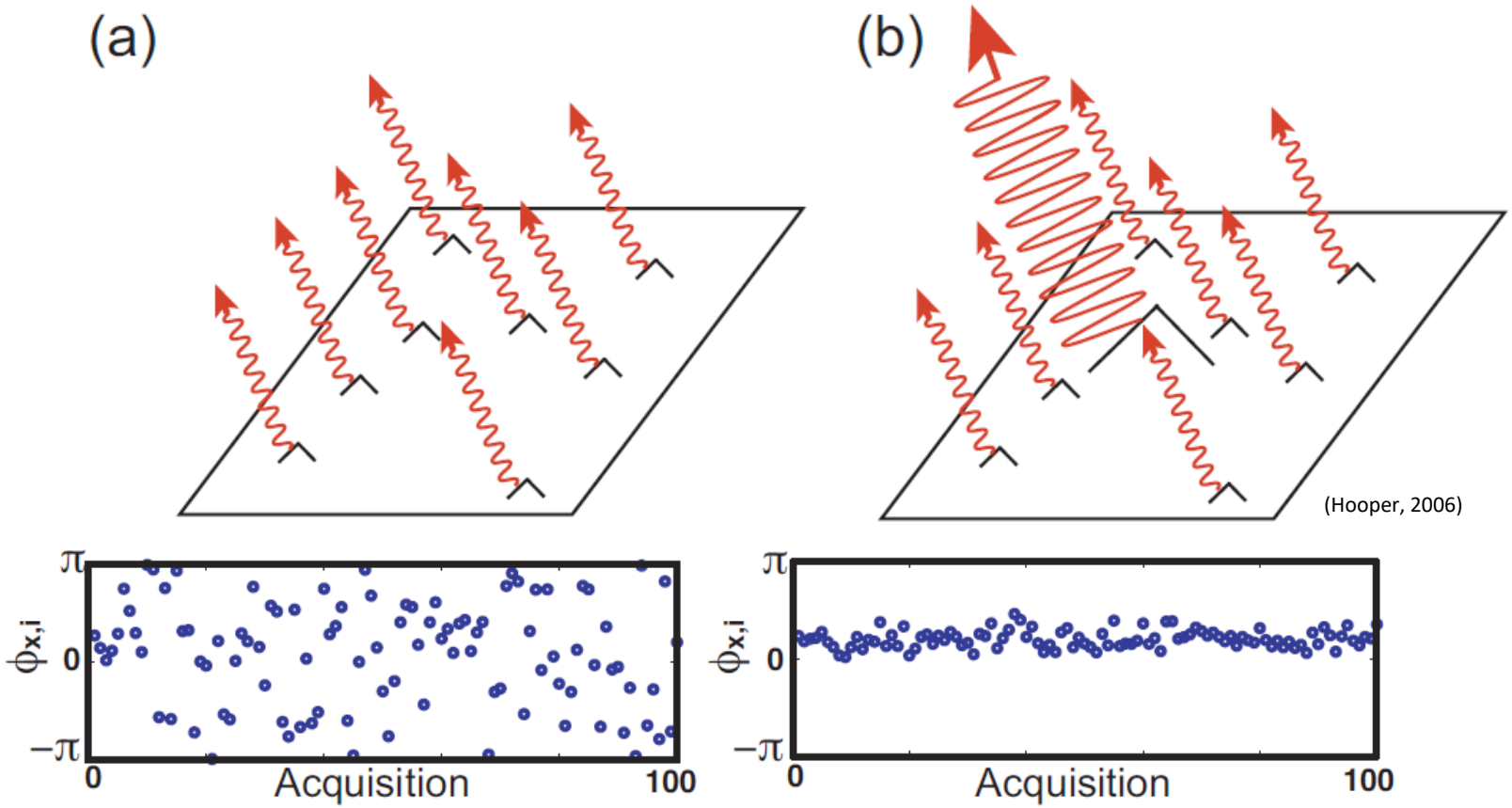

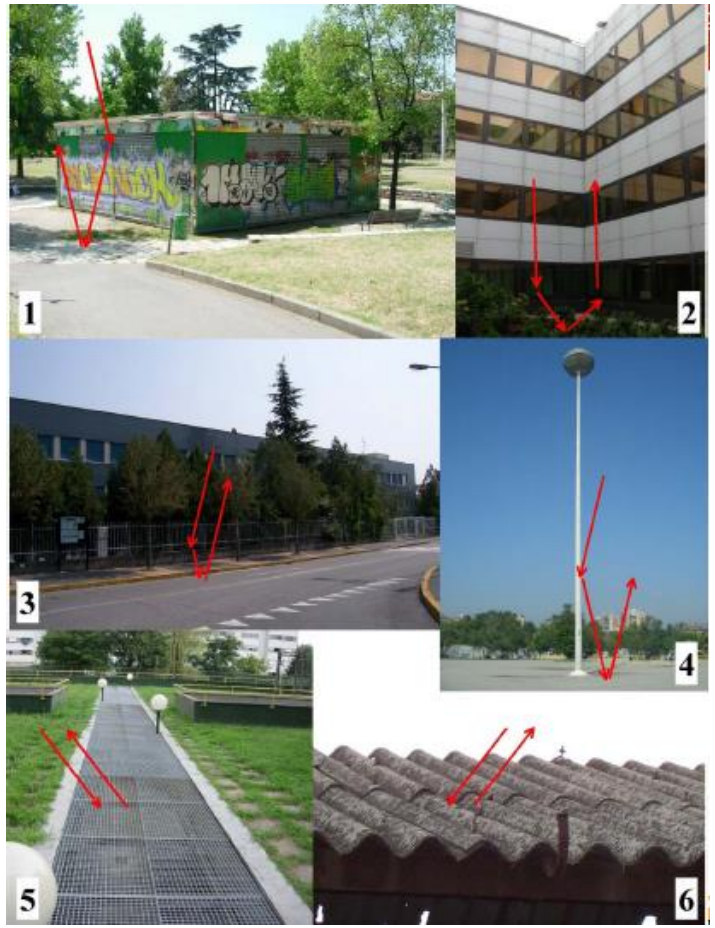

Corner Reflectors

Structures that have two or more (usually smooth) surfaces with right angles may be corner reflectors if the faces are facing the satellite.

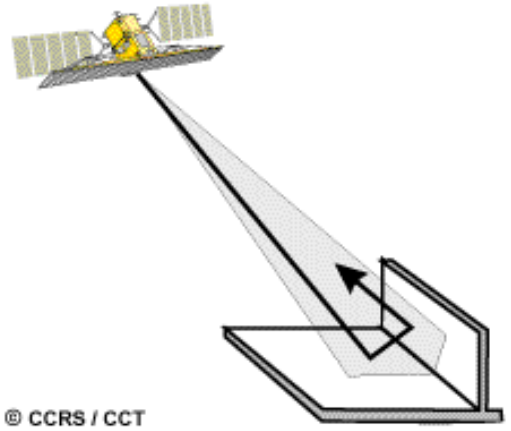

The orientation to the satellite of surfaces with a right angle between them causes most of the radar energy to be reflected directly to the antenna due to the double reflection.

In urban environments, corner reflectors with complex shapes are common. Buildings, bridges and other built structures.

FCUL

Barragem do Pizão

In 2001, Ferretti et al., proposed a technique called "Permanent Scatterers technique" that allows the analysis of long time series of interferograms.

The technique is based on a set of pixels that are consistent over time and allows, under certain conditions:

- Determining the DEM Error Used in the Differential Interferogram
- Detecting surface movements with millimetre precision

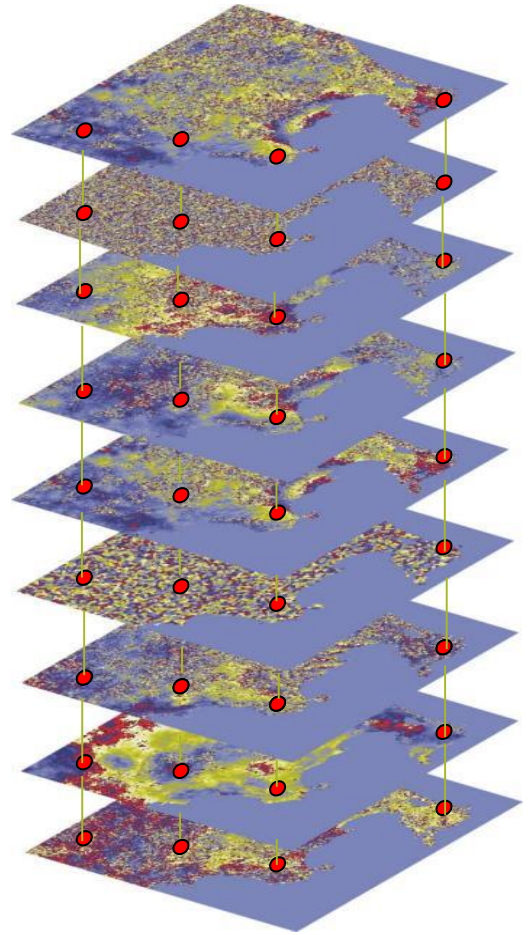

$$D_a = \frac{\sigma_a}{\bar{a}} = \hat{\sigma}_\phi$$

To estimate/mitigate atmospheric signal

To separate topography and deformation

To estimate orbit errors

To resolve the ambiguities

PERSISTENT SCATTERER

Ferretti et al., 2001,

The interferometric phase of point P of interferogram k, is:

$$\phi = \phi_{Defo} + \phi_{topo} + \phi_{atmo} + \phi_{orb} + \phi_{noise}$$

$$-\frac{4\pi}{\lambda} T^k v(x) \qquad -\frac{4\pi}{\lambda} \frac{B^k_{\perp x}}{r^m_x \sin\theta^m_{x,inc}} \cdot h_x \qquad ? \qquad -\frac{4\pi}{\lambda} \frac{B_n s}{R \tan\theta}$$

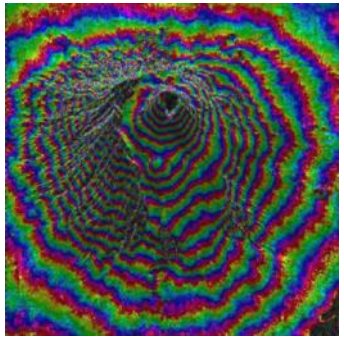

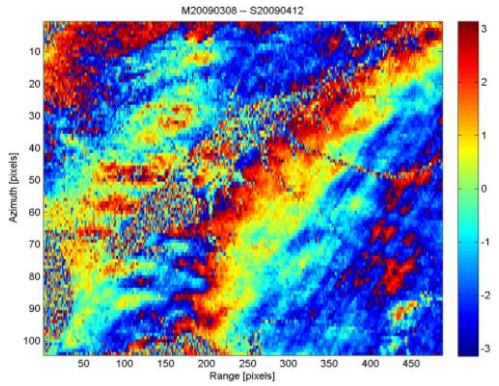

PS Processing Algorithms

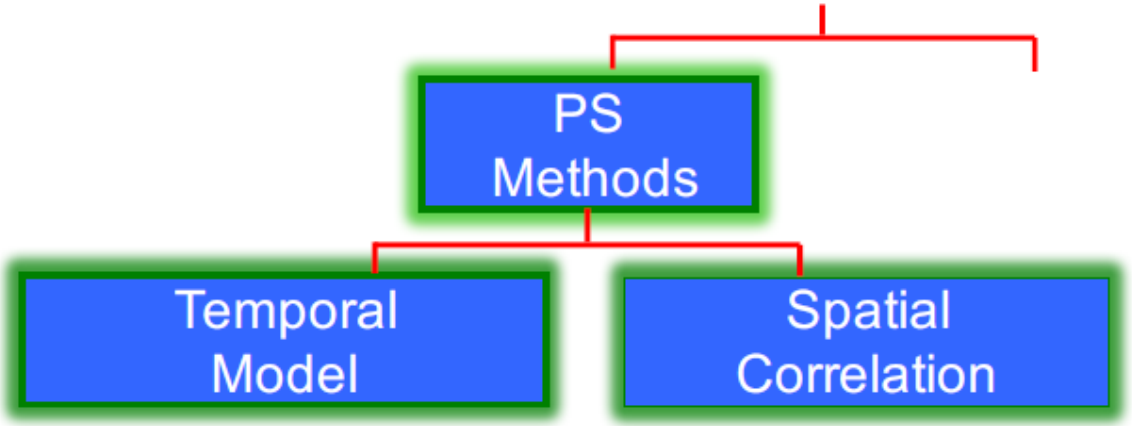

- Relying on model of deformation in time: e.g. “Permanent Scatterers” (Ferretti et al. 2001), Delft approach (Kampes et al., 2005)
- Relying on correlation in space: StaMPS (Hooper et al. 2004)

Persistent Scatter Candidates (PSC)

Ferretti et al. (2001) proposed to select a PSC if the amplitude dispersion is below a threshold, typically between 0.25 (Colesanti el al., 2003).

The amplitude dispersion index D_a is a proxy of the phase standard deviation and is defined as:

$$D_a = \frac{\sigma_a}{\bar{a}} = \hat{\sigma}_\phi$$

Where σ_a is the temporal standard deviation of the amplitude and ā the temporal mean of the amplitude for a certain pixel.

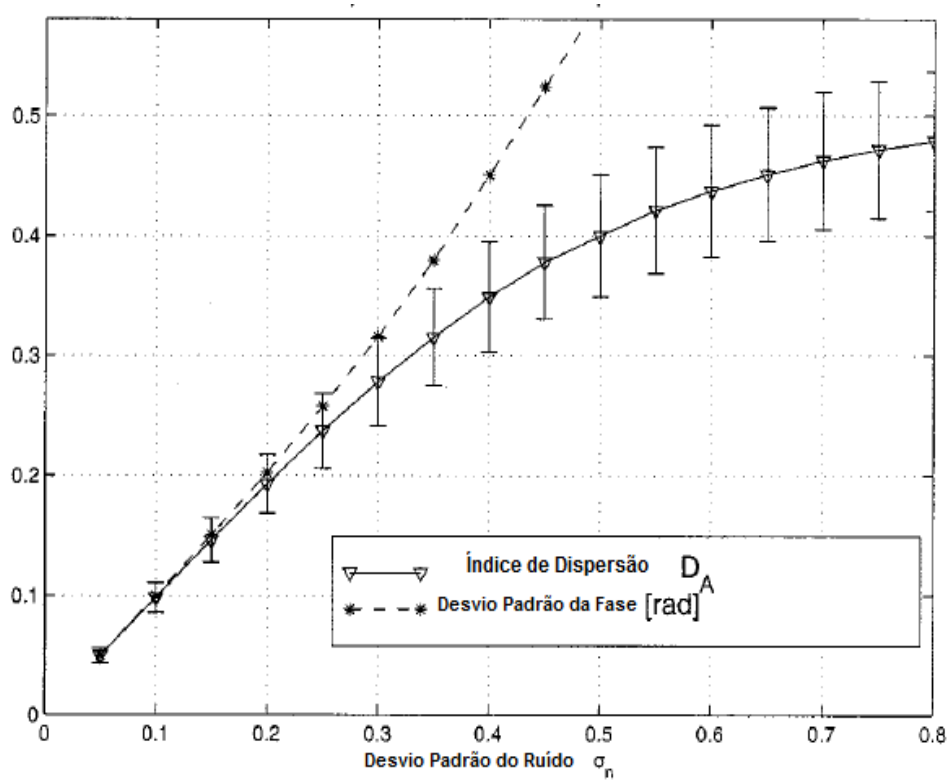

Φsat-2 begins science phase for AI Earth images

15/07/2025 3219 VIEWS 45 LIKES

ESA / Applications / Observing the Earth / Φsat-2

Φsat-2, a miniature satellite, has completed its co
delivery of science data, using algorithms to efficie
observation images, as well as detect wildfires, sh

The cubesat measuring 22 x 10 x 33 cm was launched in Augu
four days after launch. Since then, the Φsat-2 team has spent
multispectral imager and its onboard AI applications, which carry out a range of activities.

These AI capabilities include selecting images with clear visibility, while discarding images obscured by cloud cover. The algorithms can also detect and analyse disaster areas, for example zones affected by wildfires, earthquakes or floods, and identify access routes for emergency response teams. It can also be used to detect ships, gather data on illegal fishing and marine pollution. Commissioning was concluded in the second quarter of this year and the satellite is now delivering scientific data.

The satellite orbits at an altitude of 510 km. It generates images using seven multispectral bands, from visible to near-infrared, as well as one panchromatic band, with a ground sampling distance of about 5 m. This type of remote-sensing instrument is particularly useful for environmental monitoring, land management and mapping.

To mark the transition from commissioning to science phase, five images have been selected to show a range of capabilities for various end-uses over diverse types of terrain. All images are true colour using red, green and blue spectral bands, except for the image of the Bahia Blanca Estuary, which is false colour using near-infrared spectral band.

Persistent Scatter functional model

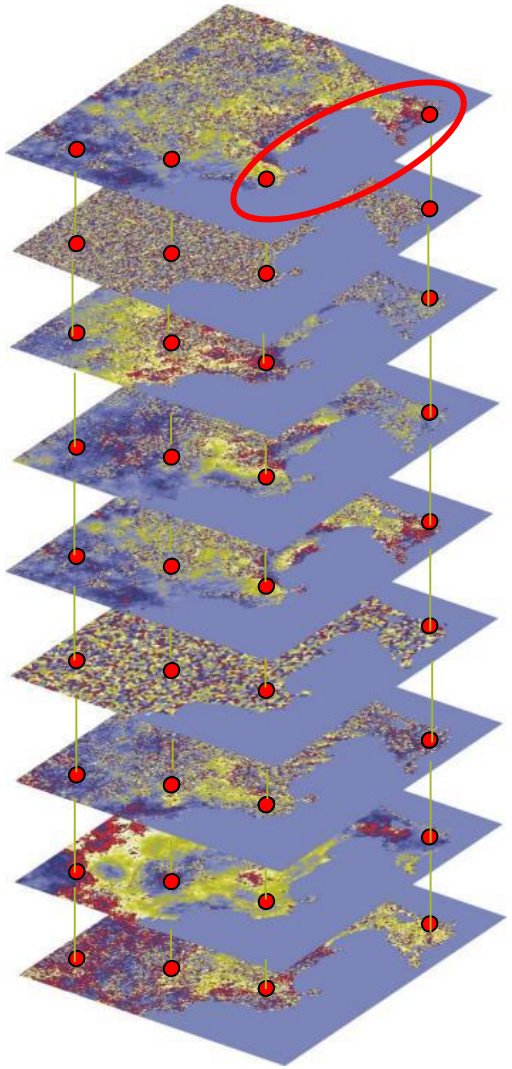

$$\phi^k = -\frac{4\pi}{\lambda} T^k v(x) - \frac{4\pi}{\lambda} \frac{B_{\perp x}^k}{r_x^m \sin \theta_{x,inc}^m} \cdot h_x + \phi_{atmo}^k + \phi_{ruido}^k$$

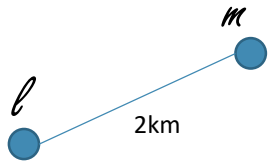

$$\Delta\phi_{l,m}^k = -\frac{4\pi}{\lambda} T^k \Delta v(x) - \frac{4\pi}{\lambda} \frac{B_{\perp x}^k}{r_x^m \sin \theta_{x,inc}^m} \cdot \Delta h_x + \omega_{l,m,k}$$

$$\Delta\phi_{l,m}^k = k_v \Delta v_{l,m} T_k + k_\varepsilon \cdot B_{n,k} \Delta h_{l,m} + \omega_{l,m,k}$$

System of k equations with 2 parameters

Search in space for the solution of values that maximize function γ

$$\gamma_{l,m} = \frac{1}{K} \sum_{k=1}^{K} \exp\left(j \cdot \left(\Delta\phi_{l,m}^k - k_v \Delta v_{l,m} T_k - k_\varepsilon \cdot B_{n,k} \Delta h_{l,m} - \omega_{l,m,k}\right)\right)$$

Integration relative to a reference

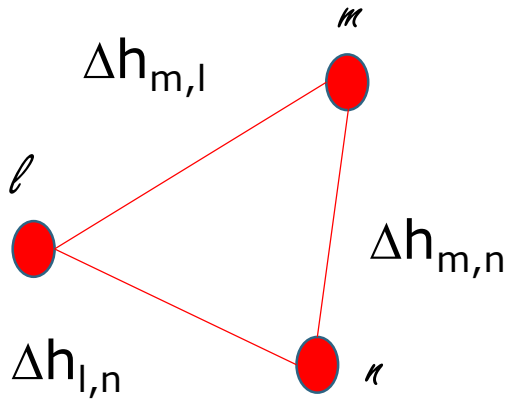

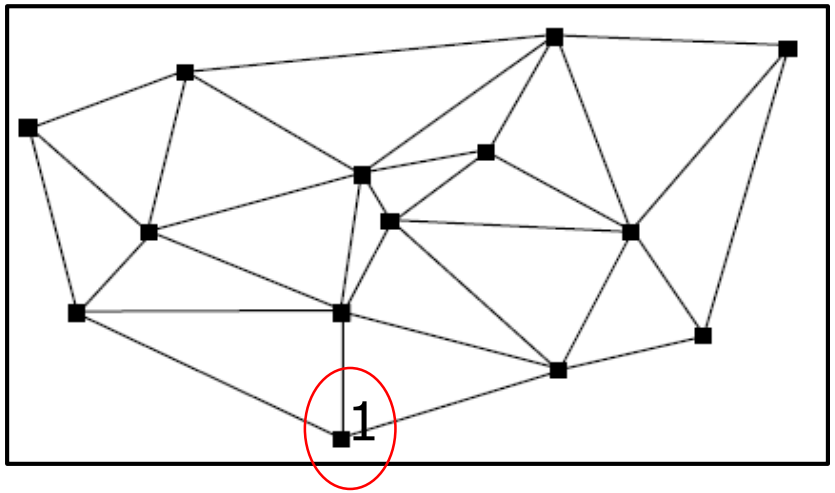

$$\begin{bmatrix} \Delta h_{2,1} \\ \Delta h_{3,1} \\ \Delta h_{4,1} \\ \vdots \\ \Delta h_{3,2} \\ \Delta h_{4,2} \\ \vdots \\ \Delta h_{H-1,H} \end{bmatrix} = \begin{bmatrix} -1 & 0 & 0 & \cdots & 0 \\ 0 & -1 & 0 & \cdots & 0 \\ 0 & 0 & -1 & \cdots & 0 \\ \vdots & & & & \\ 1 & -1 & 0 & \cdots & 0 \\ 1 & 0 & -1 & \cdots & 0 \\ \vdots & & & & \\ 0 & 0 & 0 & \cdots & -1 \end{bmatrix} \begin{bmatrix} \Delta h_2 \\ \Delta h_3 \\ \Delta h_4 \\ \vdots \\ \Delta h_{H-1} \\ \Delta h_H \end{bmatrix}$$

$$\widetilde{\Phi}_x^k = -\frac{4\pi}{\lambda} T^k v(x) - \frac{4\pi}{\lambda} \frac{B_{\perp x}^k}{r_x^m \sin \theta_{x,\mathrm{inc}}^m} \cdot h_x$$

$$e_x^k = \Phi_x^k - \left[\frac{4\pi}{\lambda} T^k v(x) - \frac{4\pi}{\lambda} \frac{B_{\perp x}^k}{r_x^m \sin \theta_{x,\mathrm{inc}}^m} \cdot h_x \right]$$

Residual phase due to atmospheric effects and non-uniform deformation.

Final estimation

The time average of the residual phase is an estimate of the atmospheric phase at the master date. Can be removed from all PSCs.

$$e'^{k}_{x} = e^{k}_{x} - \bar{e}_{x}$$

The remaining residue is successively filtered in time and space to obtain the atmospheric component of each interferogram.

$$\phi^{k}_{x,atmo} = \left[[e'^{k}_{x}]_{HP\_time} \right]_{LP\_space} + [\bar{e}_{x}]_{LP\_space}$$

APS is removed from all interferograms and the process restarted for all pixels.

Requirements

- 3 a 4 PS /km2: for interpolation of theAPS (Colesanti et al., 2003)
- 20 a 25 interferograms for the identification of PSCs with statistical significance

PSINSAR Applications: Tectonics and Subsidence

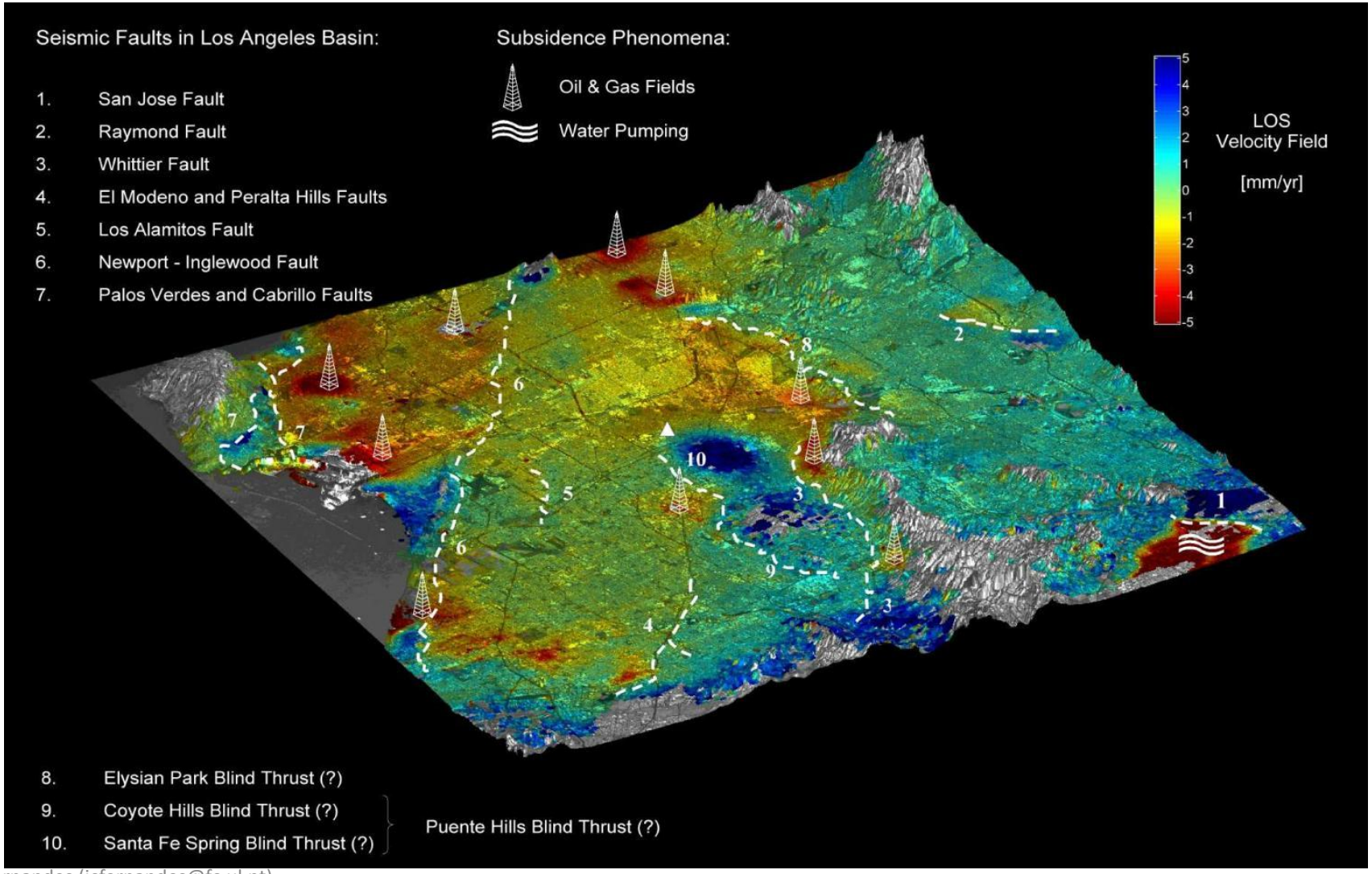

TRE, SA

Long Valley Caldera – PS InSAR

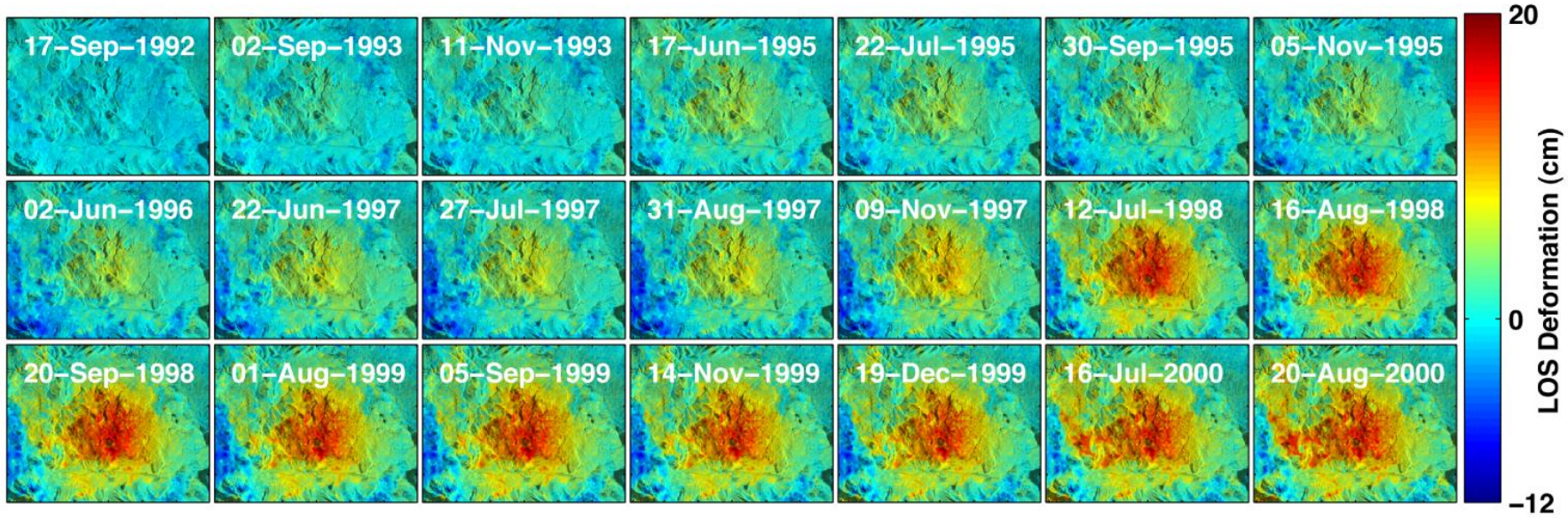

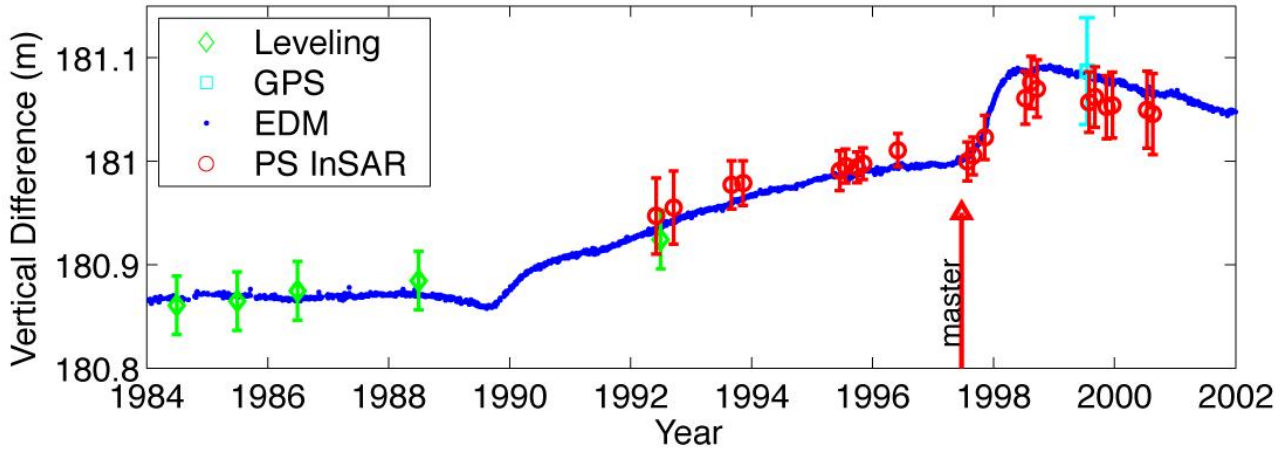

PSINSAR Applications: Subsidence (water extraction)

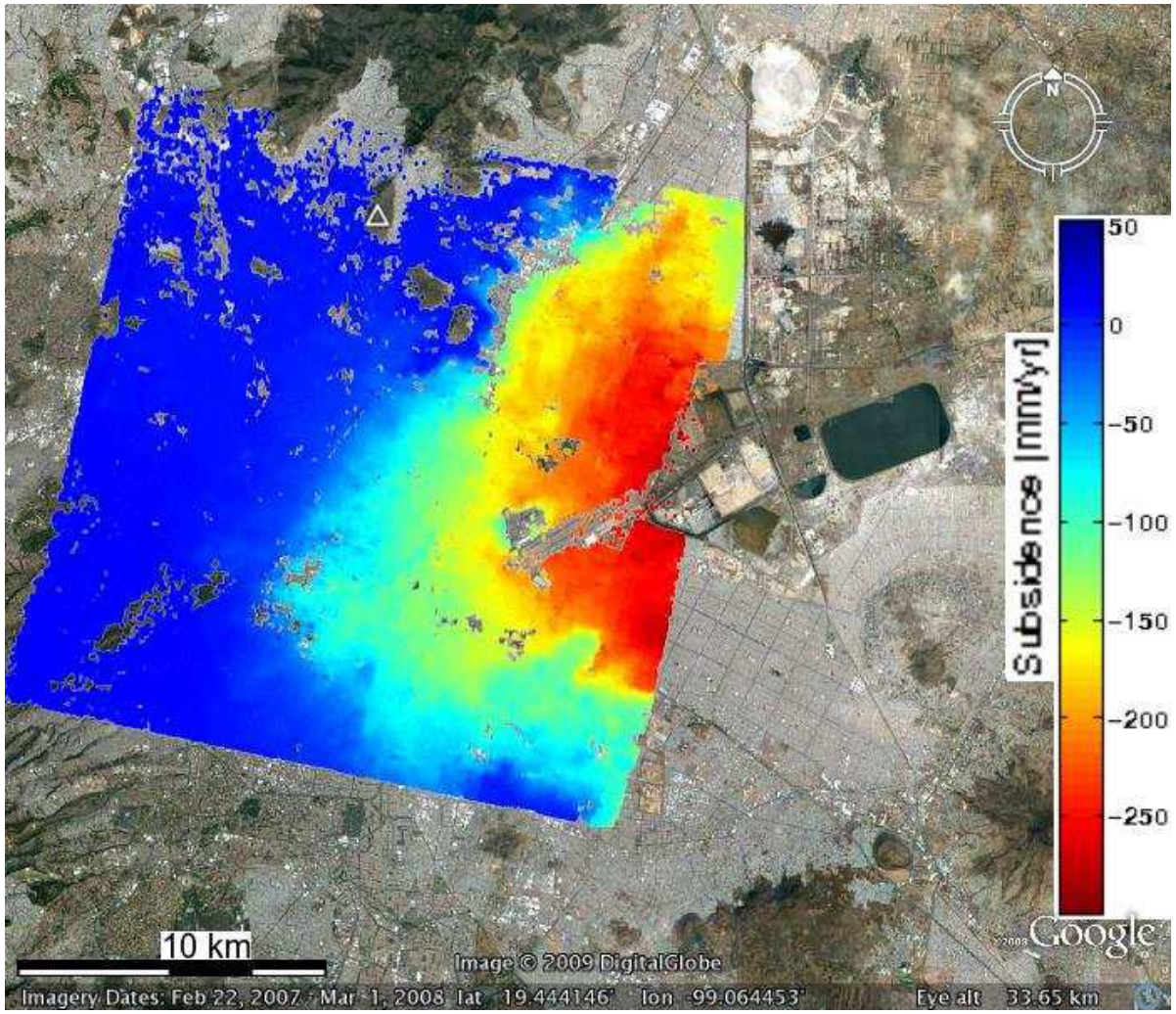

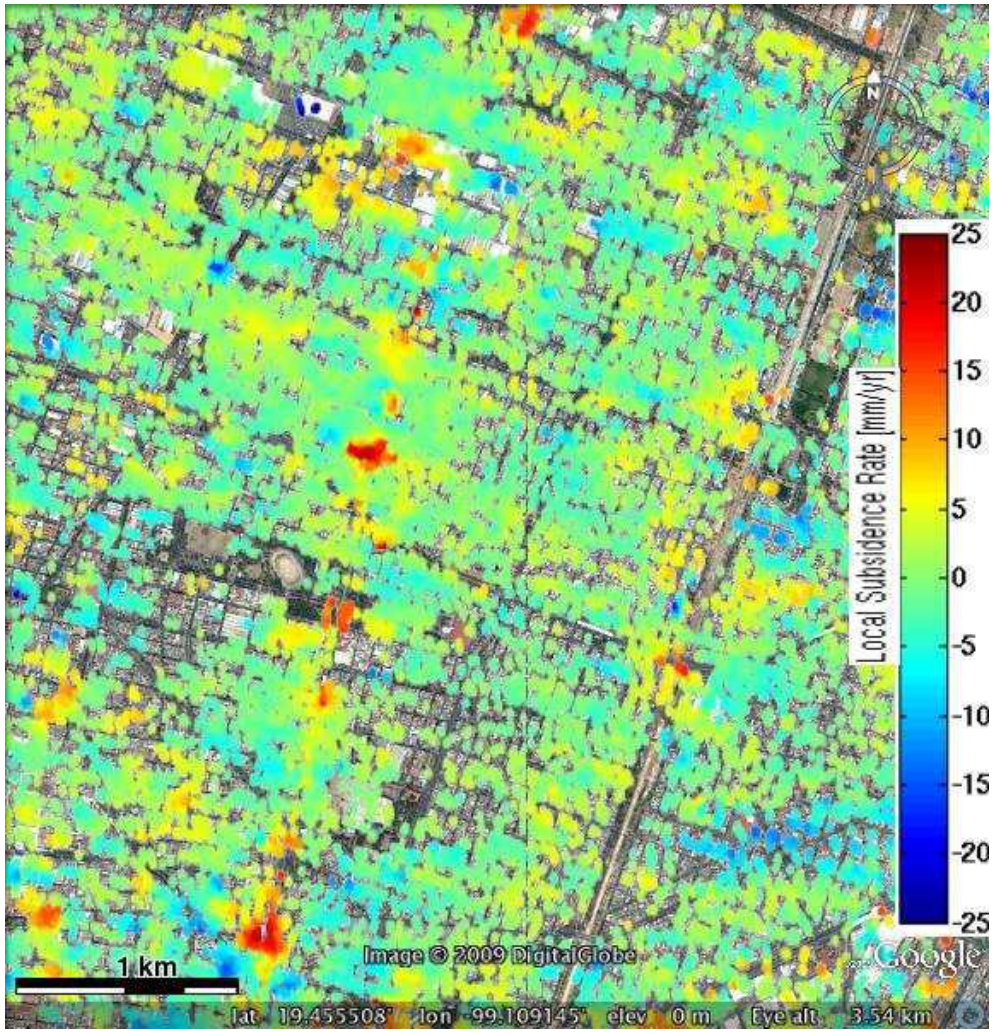

Cidade do México

Osmanoglu et al., 2011

Subsidence rates for the period 16 January 2004 to 14 July 2006 using Envisat ASAR

PSINSAR Applications: Land slides

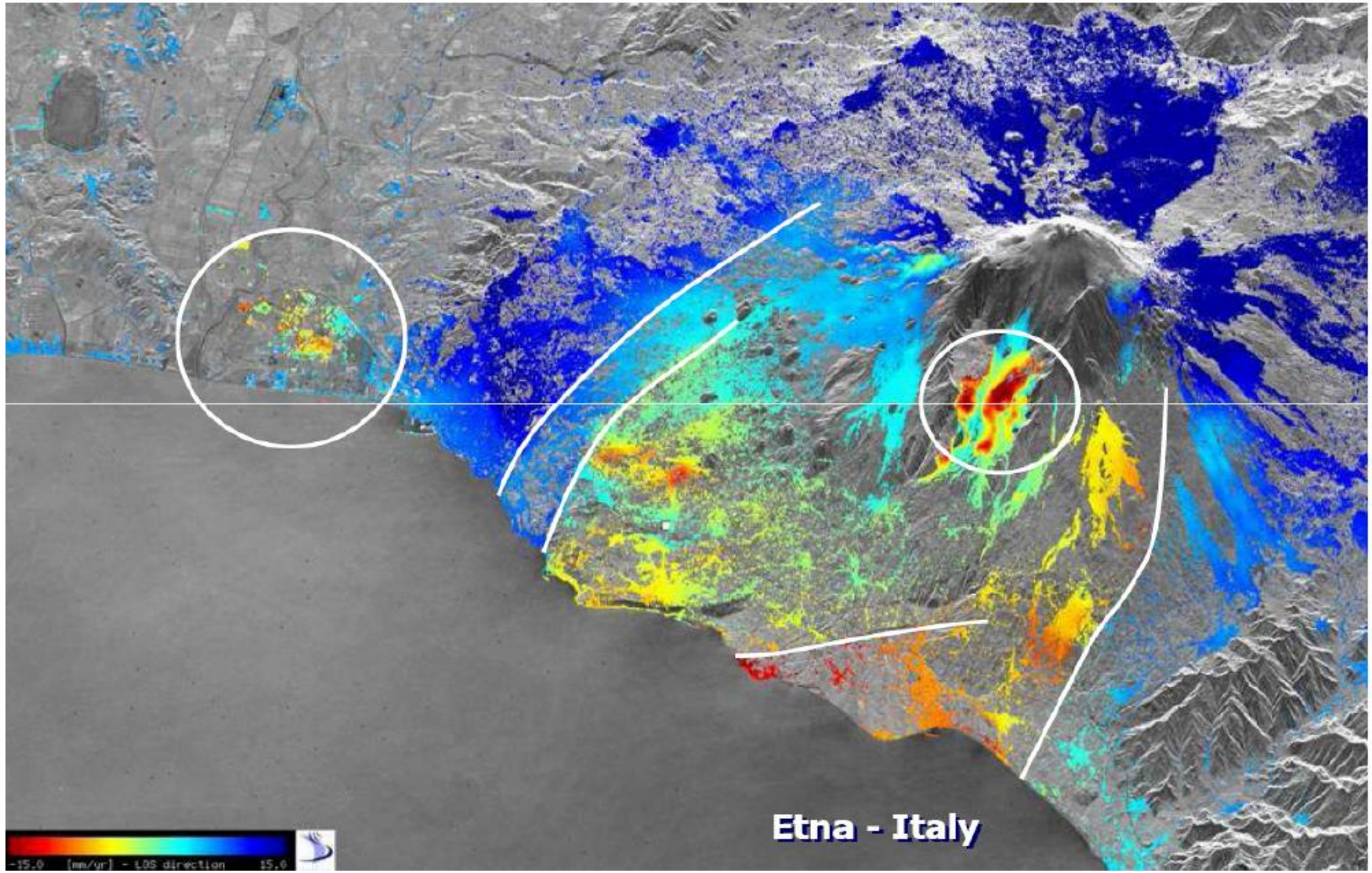

TRE, ESA

Subsidence in Lisbon(2010 – 2011), TSX

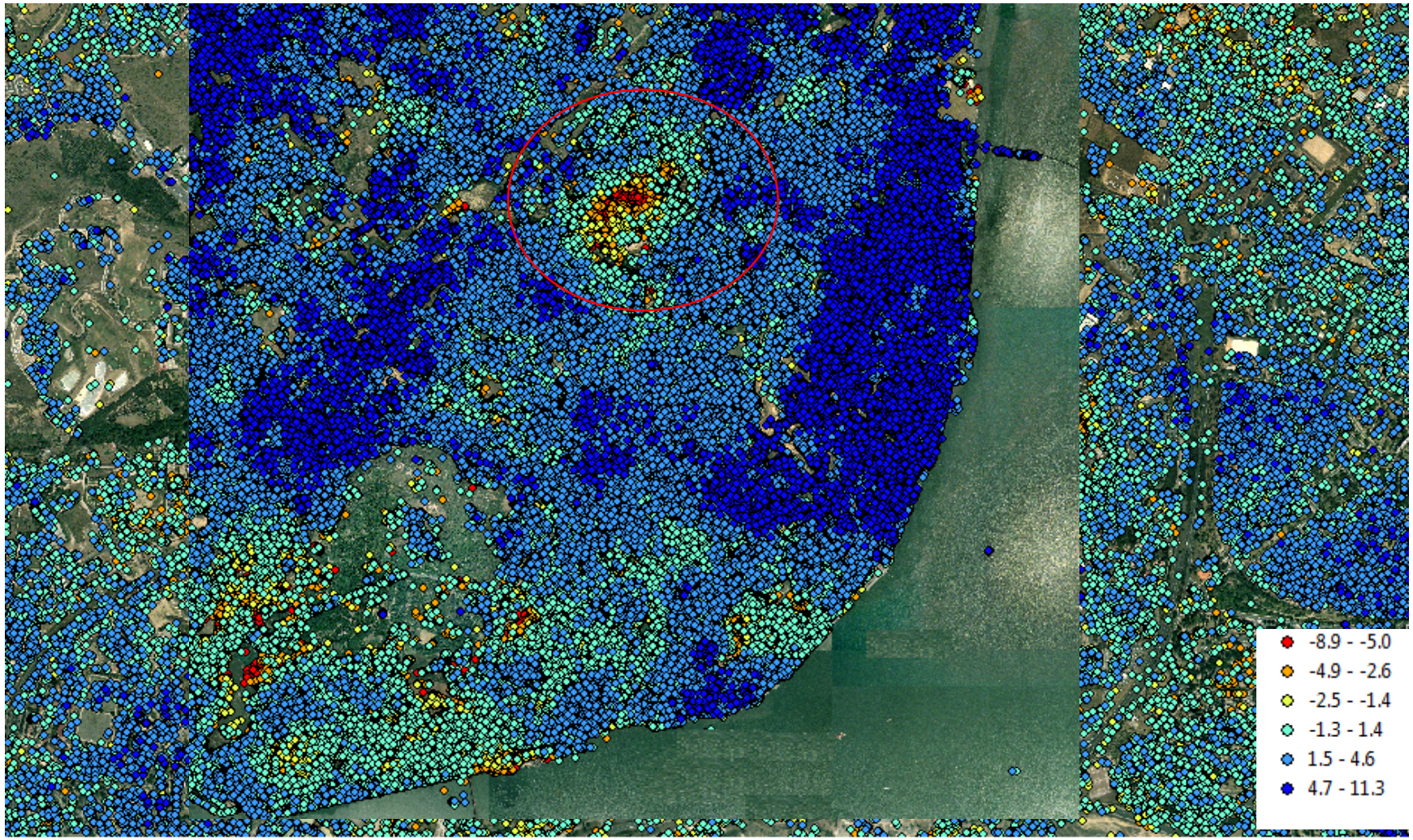

Catalão, J, et al.2011, 2015. Detection of ground subsidence in the city of Lisbon: comparison of InSAR and topographic measurements.

PSINSAR Applications: Digital Surface Model

Crosetto, M., Monserrat, O., Iglesias, R. and Crippa, B., 2010.

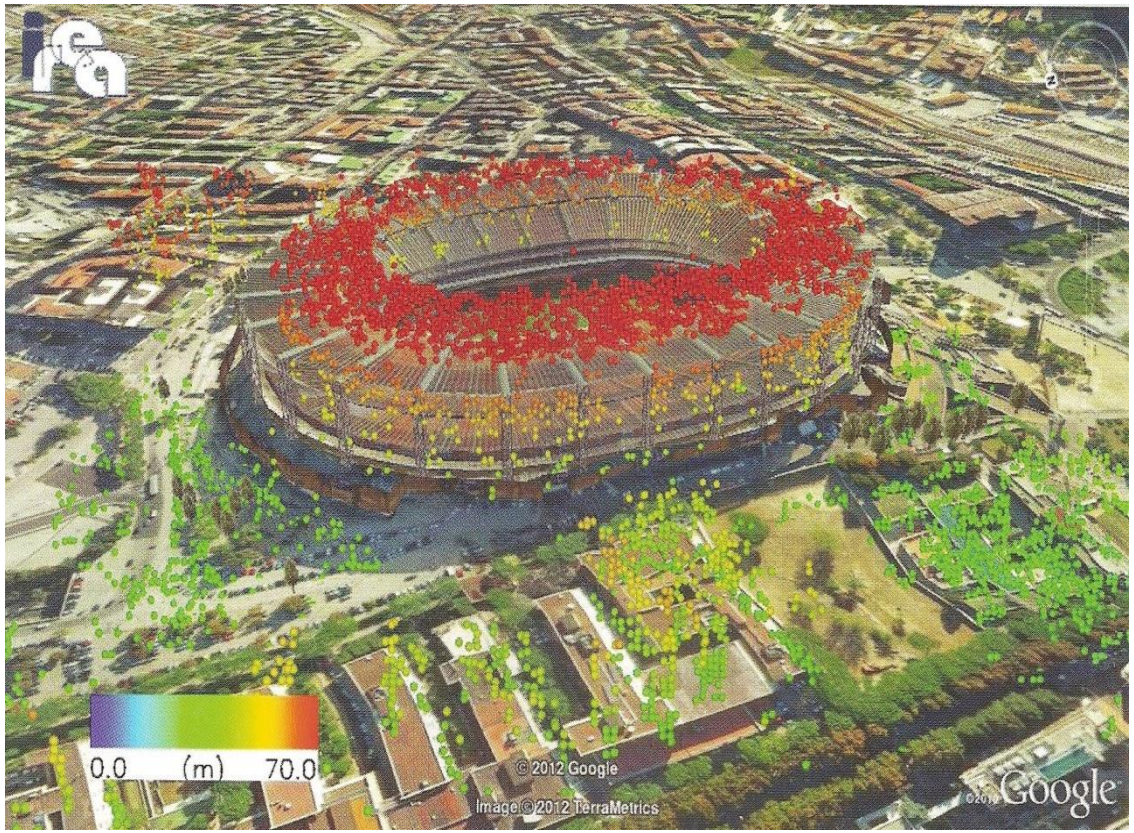

Zhu and Bamler, 2010

Limitations of the technique

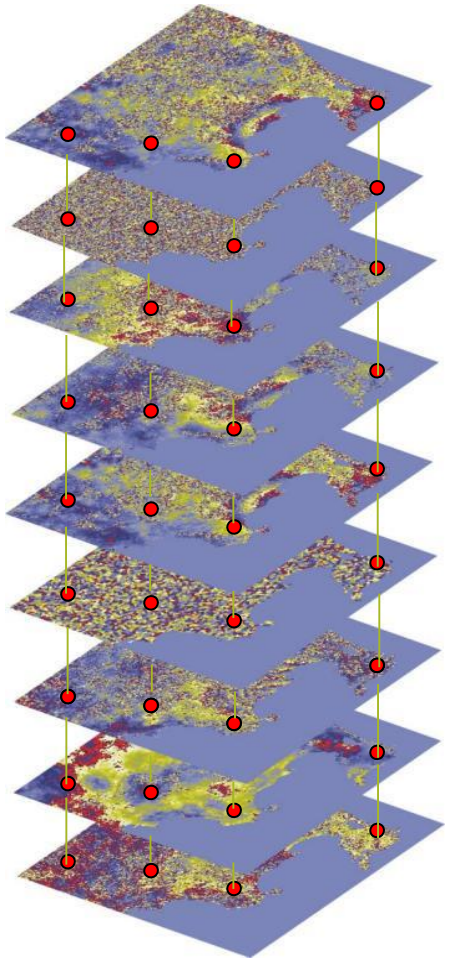

1

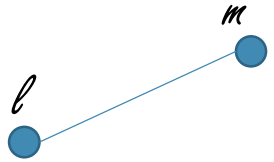

Distance between PSC < 2 km

In natural environments this condition is not verified.

2

The PS must obey a predefined deformation model, linear in time.

Many of the deformation processes follow non-linear processes in time (landslides, volcanism)

Hooper et al. (2004) proposes a method based on phase analysis and spatial correlation of phases, as an alternative to a pre-defined strain model.

Explores the spatial correlation of the deformation signal.

The Ferretti method assumes a linear deformation model

StaMPS PS Approach

Developed for more general applications, to work:

a) in rural areas without buildings (low amplitude)

b) when the deformation rate is very irregular

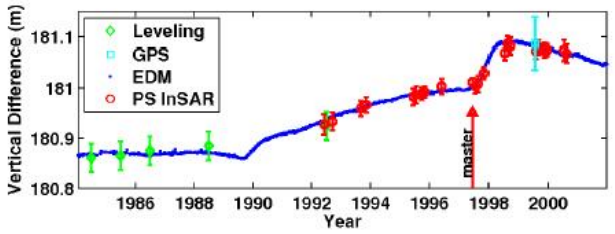

Phase Analysis

The phase of a pixel x in the interferogram k is given by:

$$\psi_x^k = W\{\phi_{x,def.}^k + \phi_{x,atmo}^k + \phi_{x,orb}^k + \phi_{x,\theta}^k + \phi_{x,noise}^k\}$$

The correlated part of the signal is estimated using an average filter in the frequencies domain and removed from the original signal:

$$\psi_x^k - \tilde{\psi}_x^k = W\left\{\frac{4\pi}{\lambda} \mathrm{B}_{\perp,\mathrm{x}}^{\mathrm{k}} \Delta\theta_x^u + \phi_{x,noise}^{k,u} + \Delta_x\right\}$$

Nonlinear Equation Due to Coiled Phase

u designates the spatially uncorrelated part.

Hooper defined the standard for the variation of the residual phase of a pixel as:

$$\gamma_x = \frac{1}{K}\left|\sum_{k=1}^{K} \exp(j(\psi_x^k - \tilde{\psi}_x^k - \Delta\tilde{\phi}_{x,\theta}^{k,u}))\right|$$

The value of the topographic phase is selected by maximizing this standard.

γ_x is a measure of the phase noise level and an indication of the pixel phase stability, used to determine whether a pixel is a PS.

Seleção dos PS

Knowing the value of γ_x for each pixel

Determine value γ^* that maximizes the probability of pixel x being PS

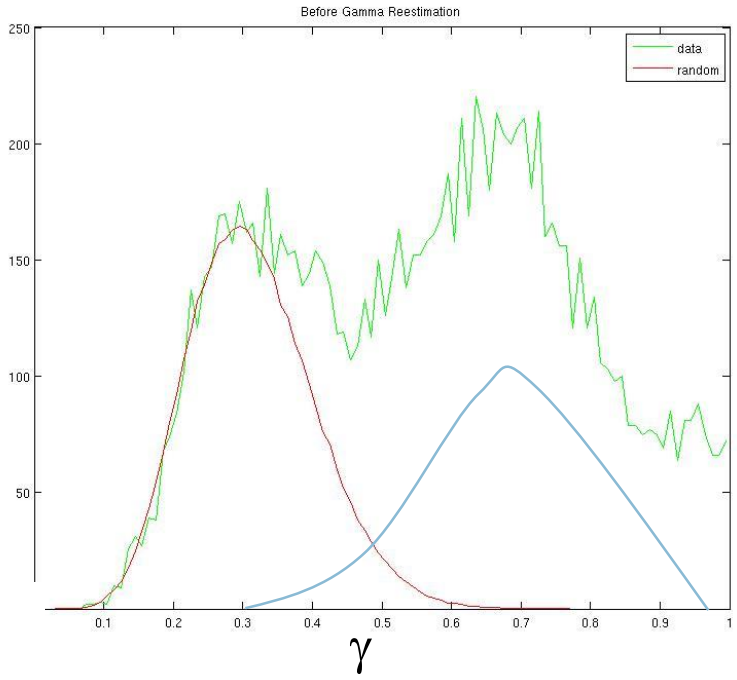

$$q = \frac{(1-\alpha)\int_{\gamma^*}^{1} p_R(\gamma_x)d\gamma_x}{\int_{\gamma^*}^{1} p(\gamma_x)d\gamma_x} \Rightarrow \gamma^*$$

q: is the probability of selecting false PS

$(D_{A,x}, \gamma_x^*)$ →

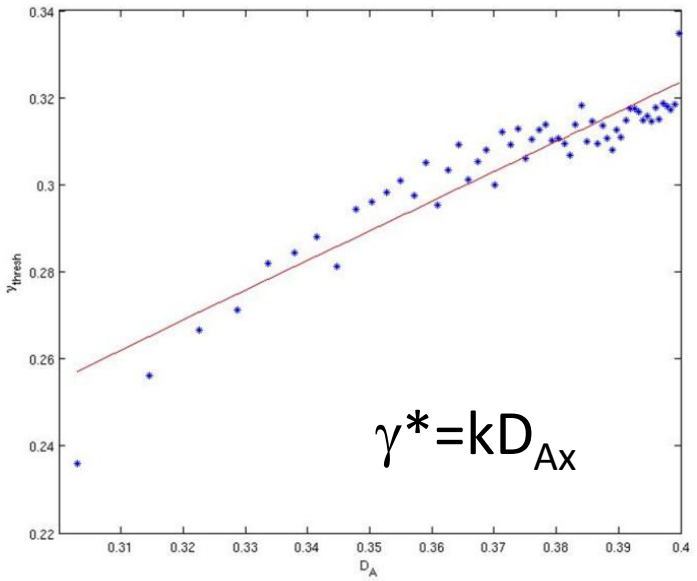

Finding the constant of proportionality k

It will be PS any pixel that checks the interface:

$$\gamma_x > k\, D_{A,x}$$

PS Selection (after)

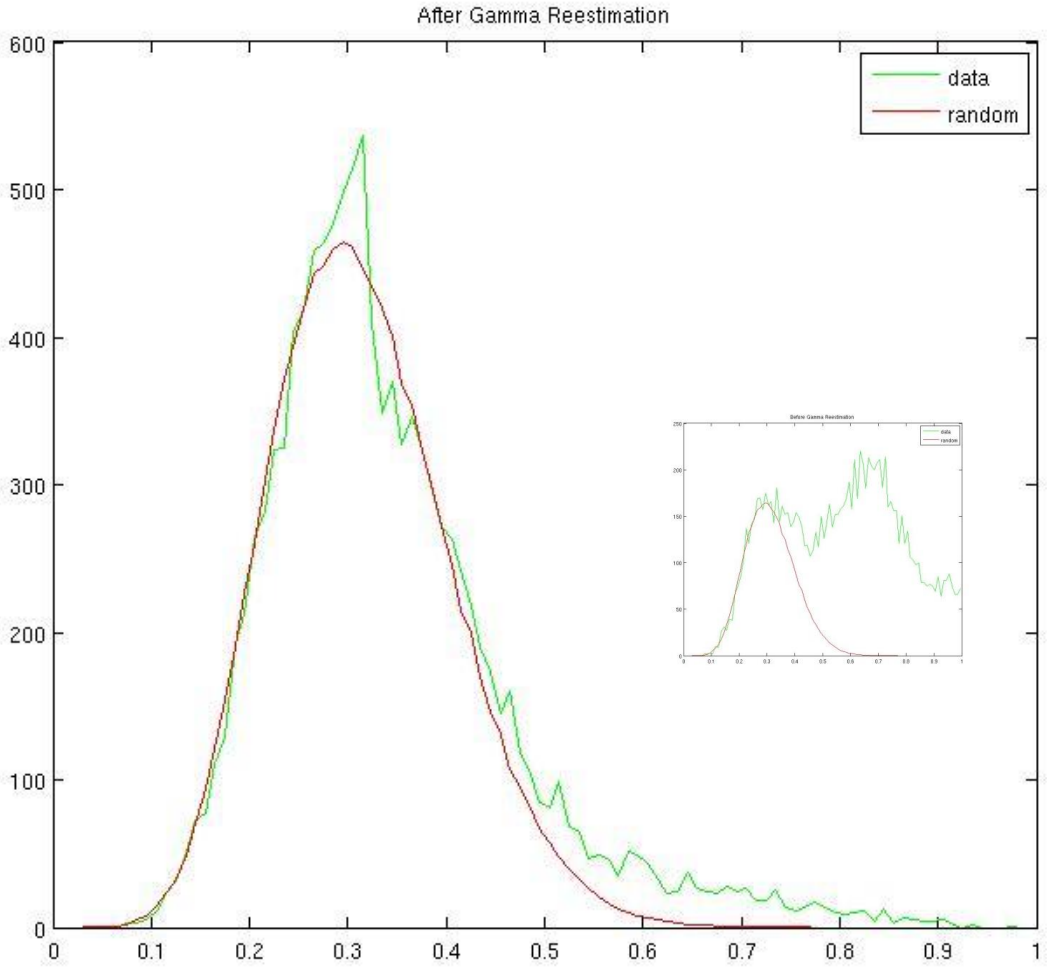

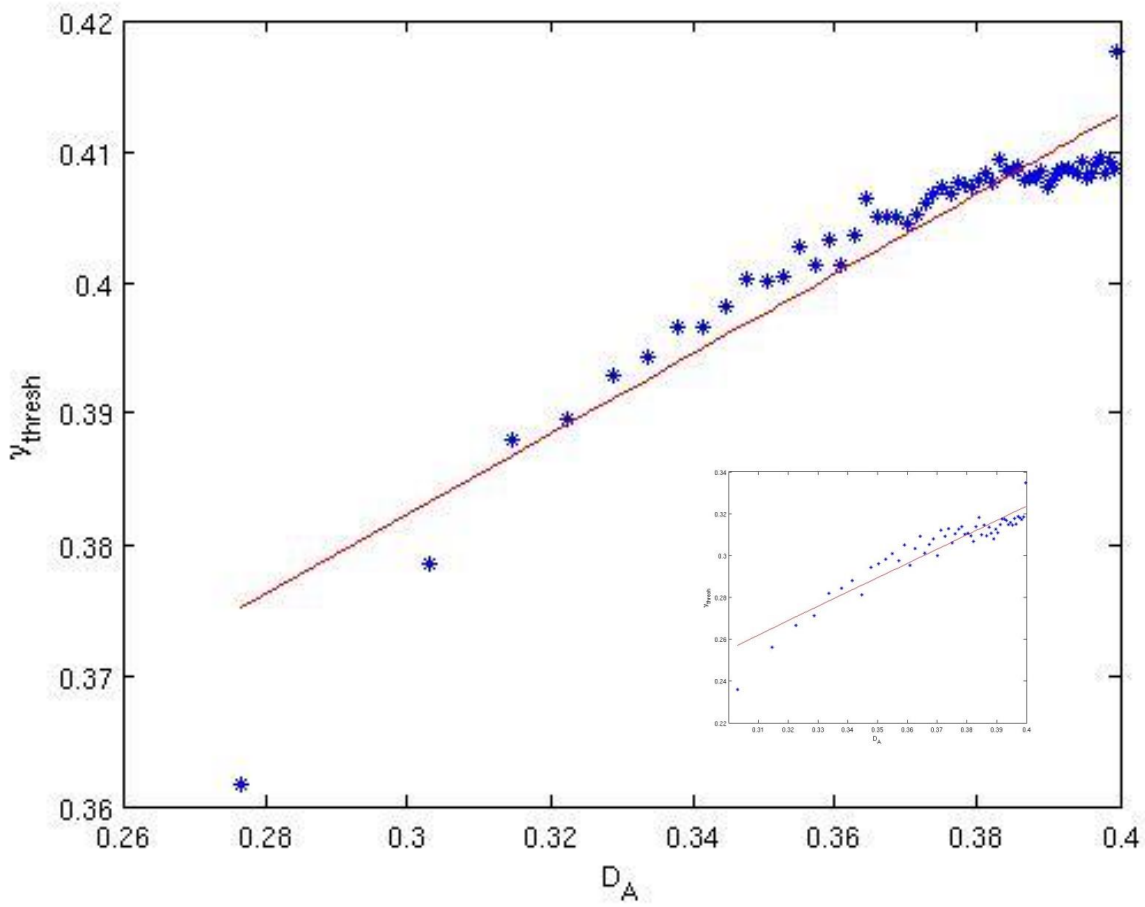

Strategies for combining SAR images

Everyone with Everyone

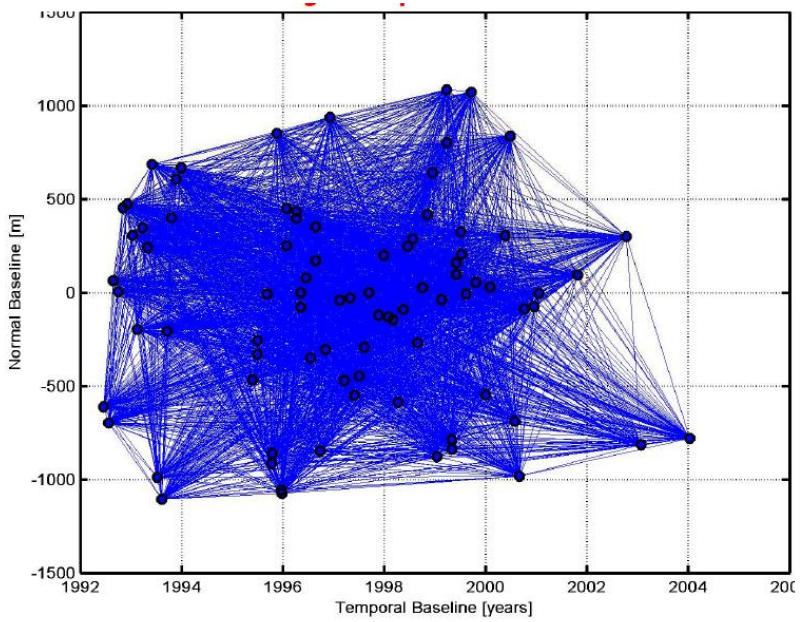

Temporal baseline minimization

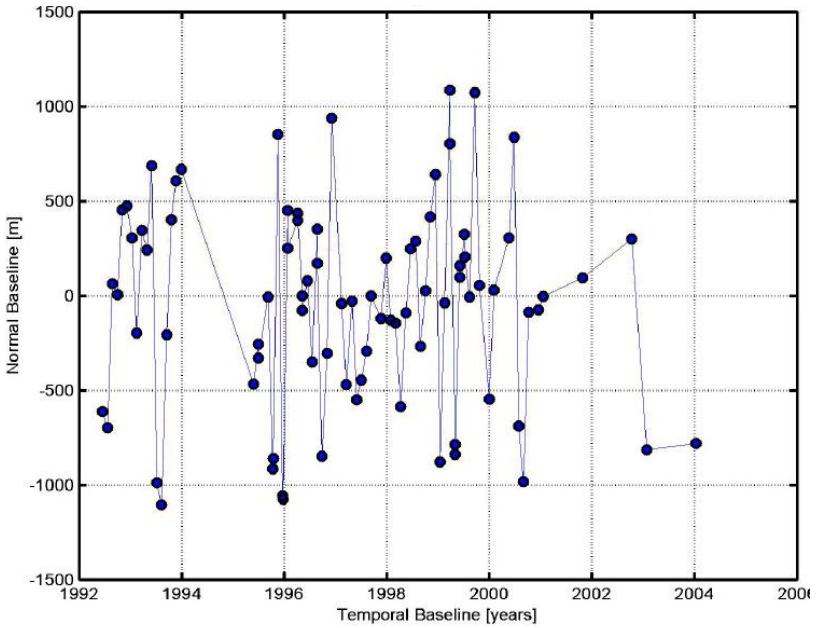

PS analysis

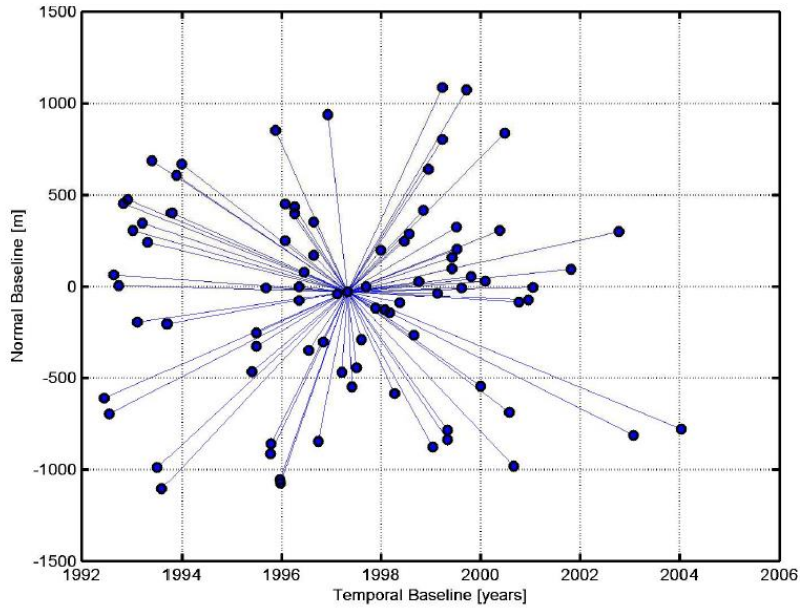

Persistent Scatterers (Hooper)

Marques, F.O., **Catalão, J.**, Hildenbrand, A, Madureira, P., 2015. Tectonophysics

Limitations of the PSInSAR technique

… In a geodesic perspective

(measurement of the Earth's gravitational shape and field and its temporal variations)

Time series limited to the lifetime of the satellite.

Randomness in the location of the PSs

Lack of definition of the coordinated reference system

Need for a high number of images (over 20)

Satellite line-of-sight (LOS) measurement

Insufficient modelling of atmospheric effects

Functional Model + Stocastic Model

STUN, Bert Kampes, 2006

Deformation and Phase

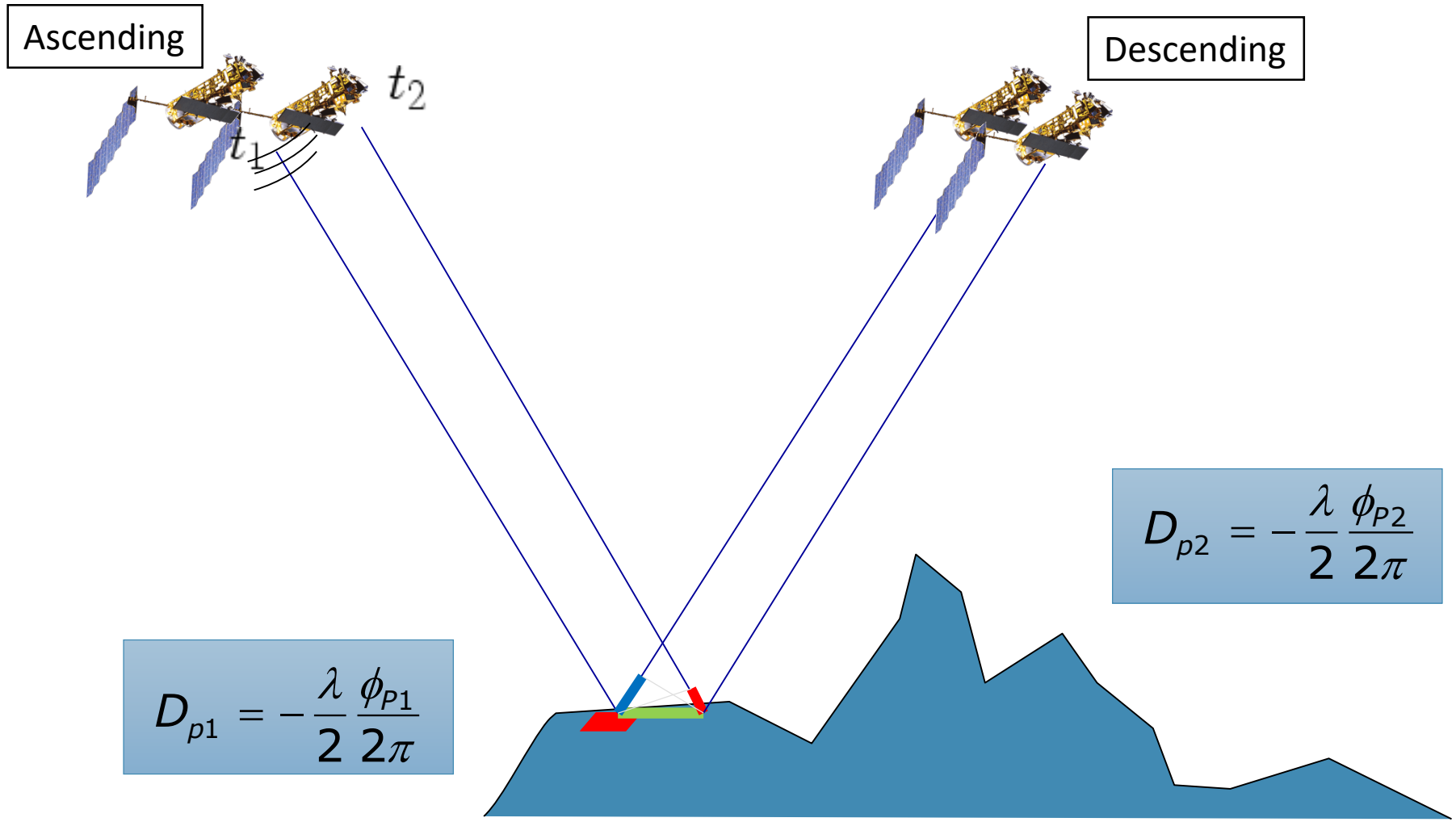

InSAR displacement decomposition

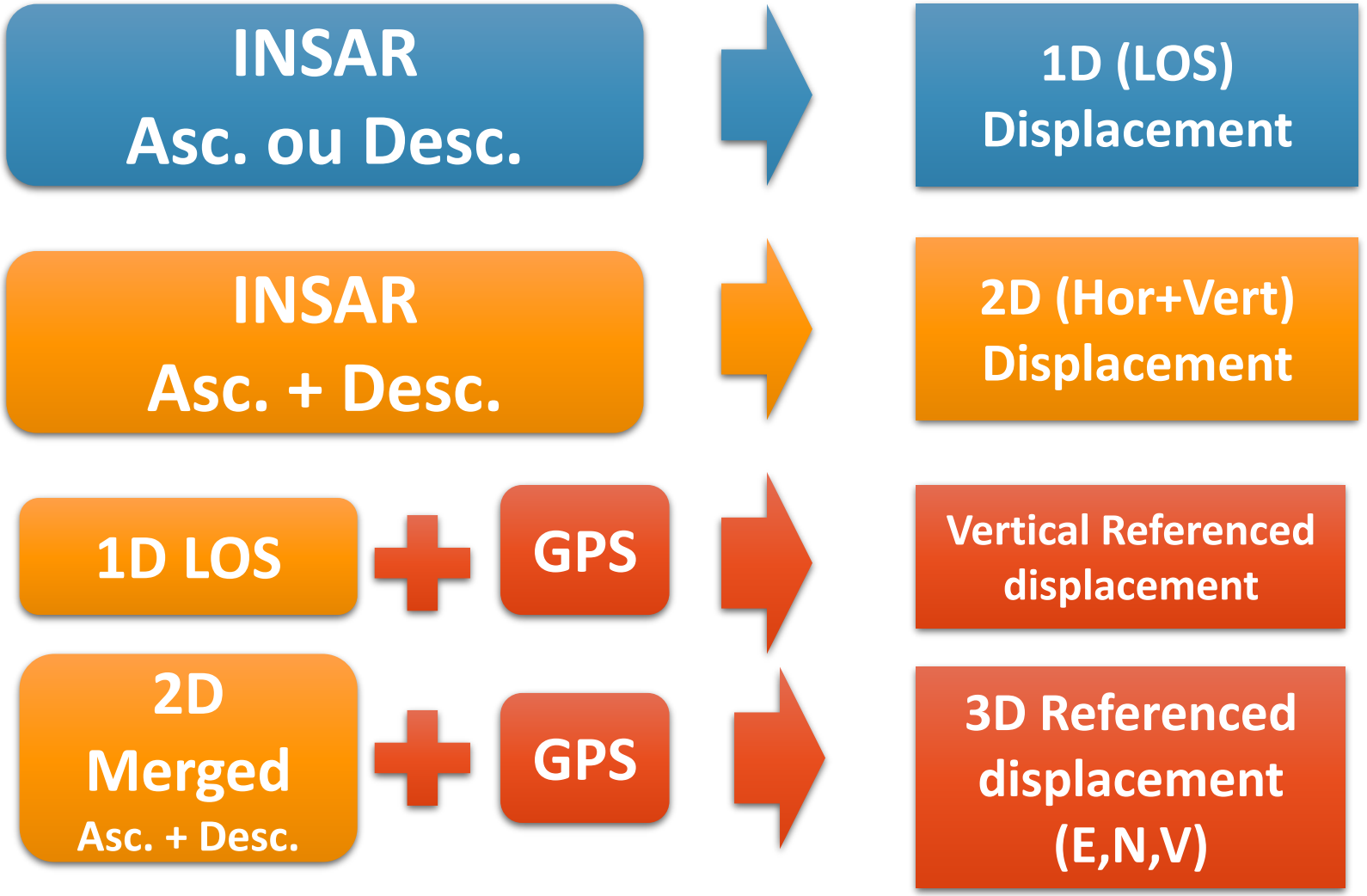

Displacement 2D (horizontal + vertical)

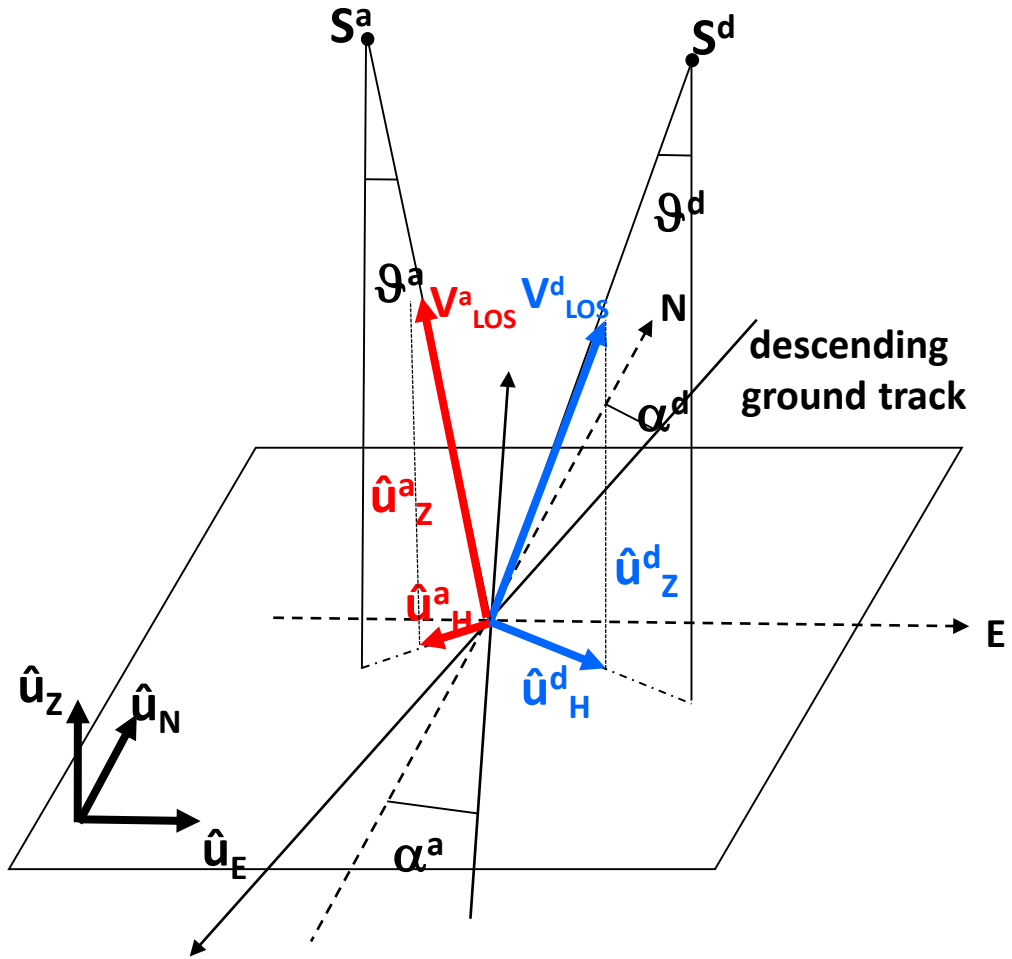

$$V_{LOS} = (V_E, V_N, V_Z) \cdot (u_E, u_N, u_z)$$

$$\begin{cases} V^a_{LOS} = (V_E, V_N, V_Z) \cdot (u^a_E, u^a_N, u^a_z) \\ V^d_{LOS} = (V_E, V_N, V_Z) \cdot (u^d_E, u^d_N, u^d_z) \end{cases}$$

$$\begin{cases} V^d_{LOS} = V_H u^d_H + V_Z u^d_z \\ V^a_{LOS} = V_H u^a_H + V_Z u^a_z \end{cases}$$

$$\Rightarrow \quad (V_H, V_Z)$$

Integration with GPS

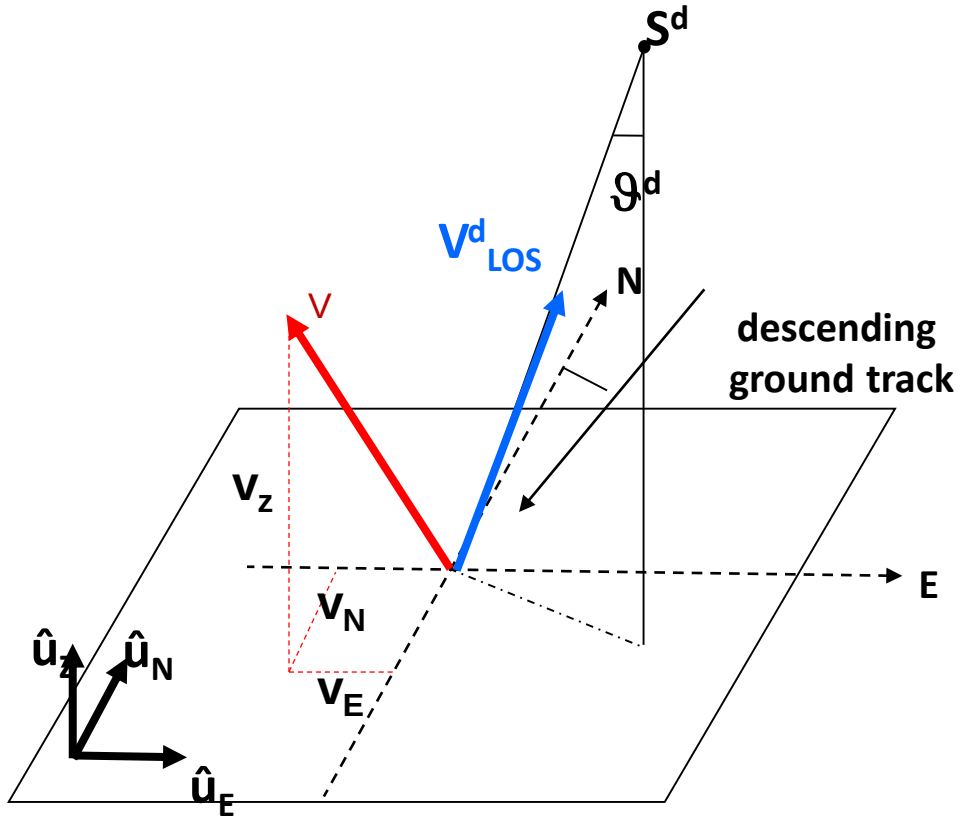

$$V_{LOS} = (V_E, V_N, V_Z) \cdot (u_E, u_N, u_z)$$

$$\mathbf{V}_{LOS} = v_E u_e + v_N u_n + v_Z u_z$$

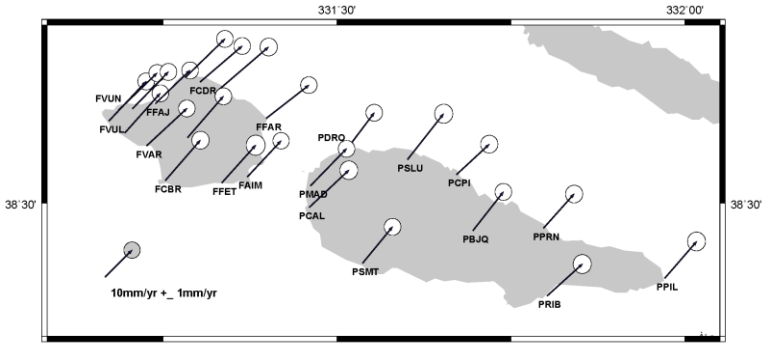

$$v_z = \frac{1}{u_z}(V_{LOS} - \hat{v}^e_{GPS} u_e - \hat{v}^n_{GPS} u_n) \quad (V_H u^d_H)$$

$$E = \sum_{i=1}^{N_{GPS}} \left\{ \mu(v^z_{LOS})(i) + D - v^z_{GPS}(i) \right\}^2$$

Catalão, et al., 2011.

PS LOS velocity - Descending

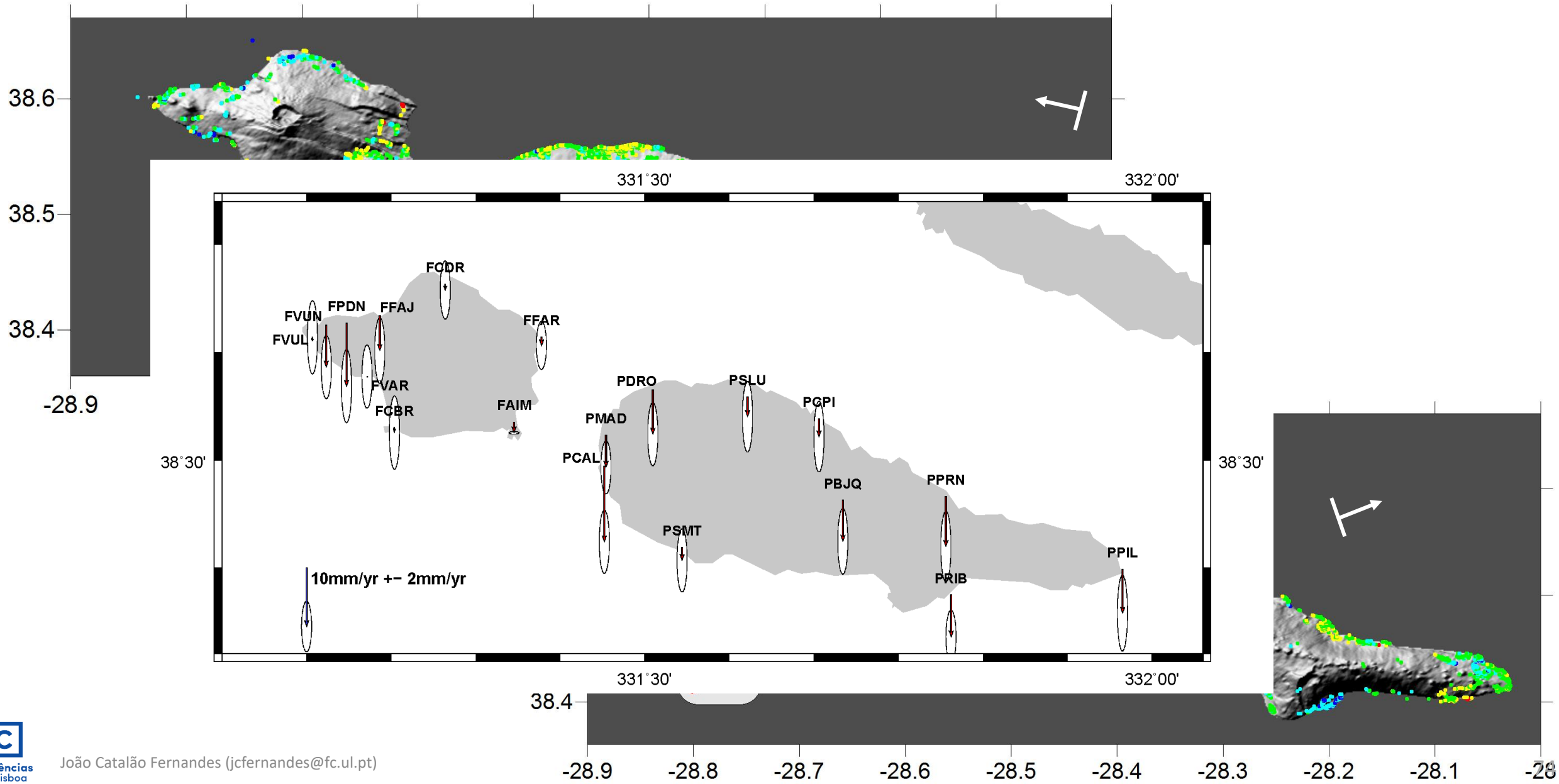

Vertical velocity ITRF2008 (2007-2009)

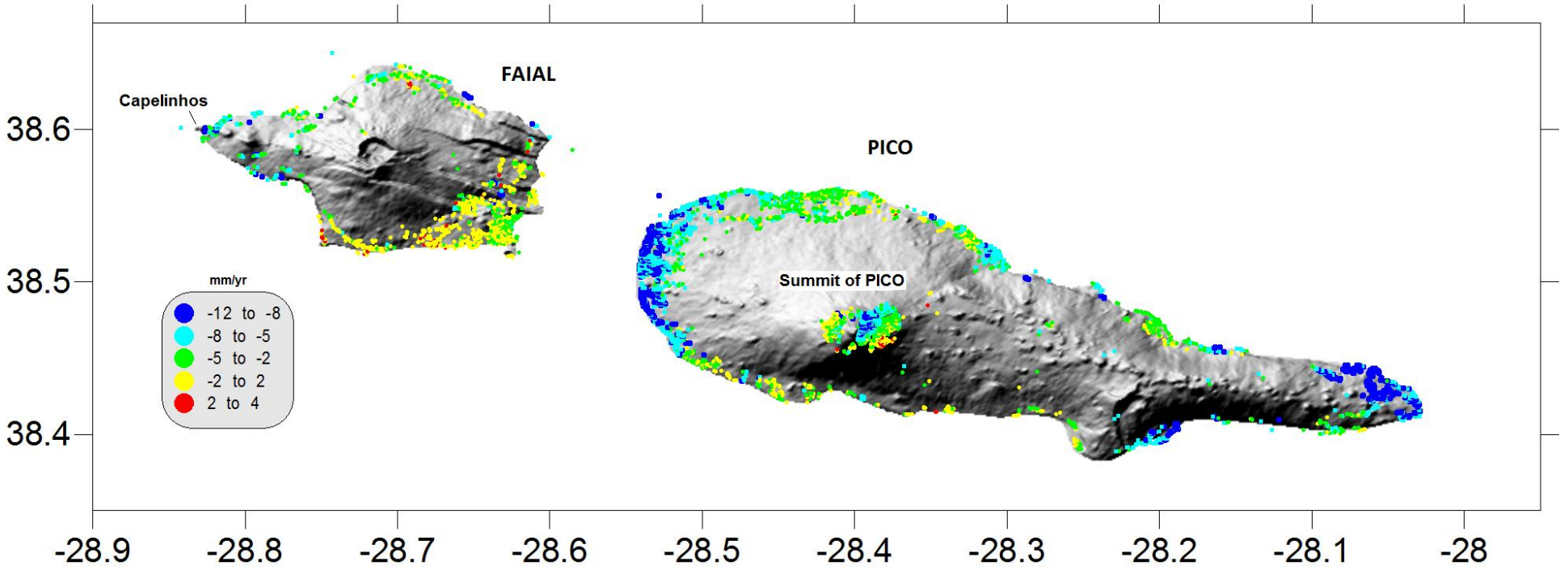

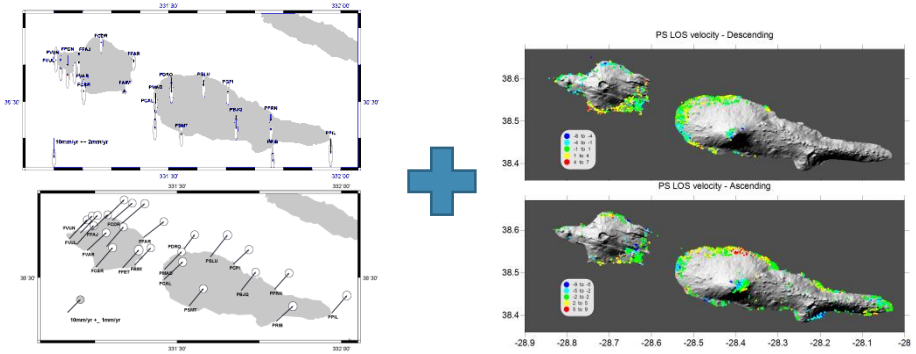

$$E = \sum_{i=1}^{N_{GPS}} \left\{ \mu(v_{PS}^{v})(i) + D(\varphi,\lambda) - v_{GPS}^{v}(i) \right\}^2$$

$$D(\varphi,\lambda) = \alpha\, cos\varphi cos\lambda + \beta\, cos\varphi sin\lambda + \gamma\, sin\varphi + \delta$$

Catalão el al., 2011

Atmospheric effects

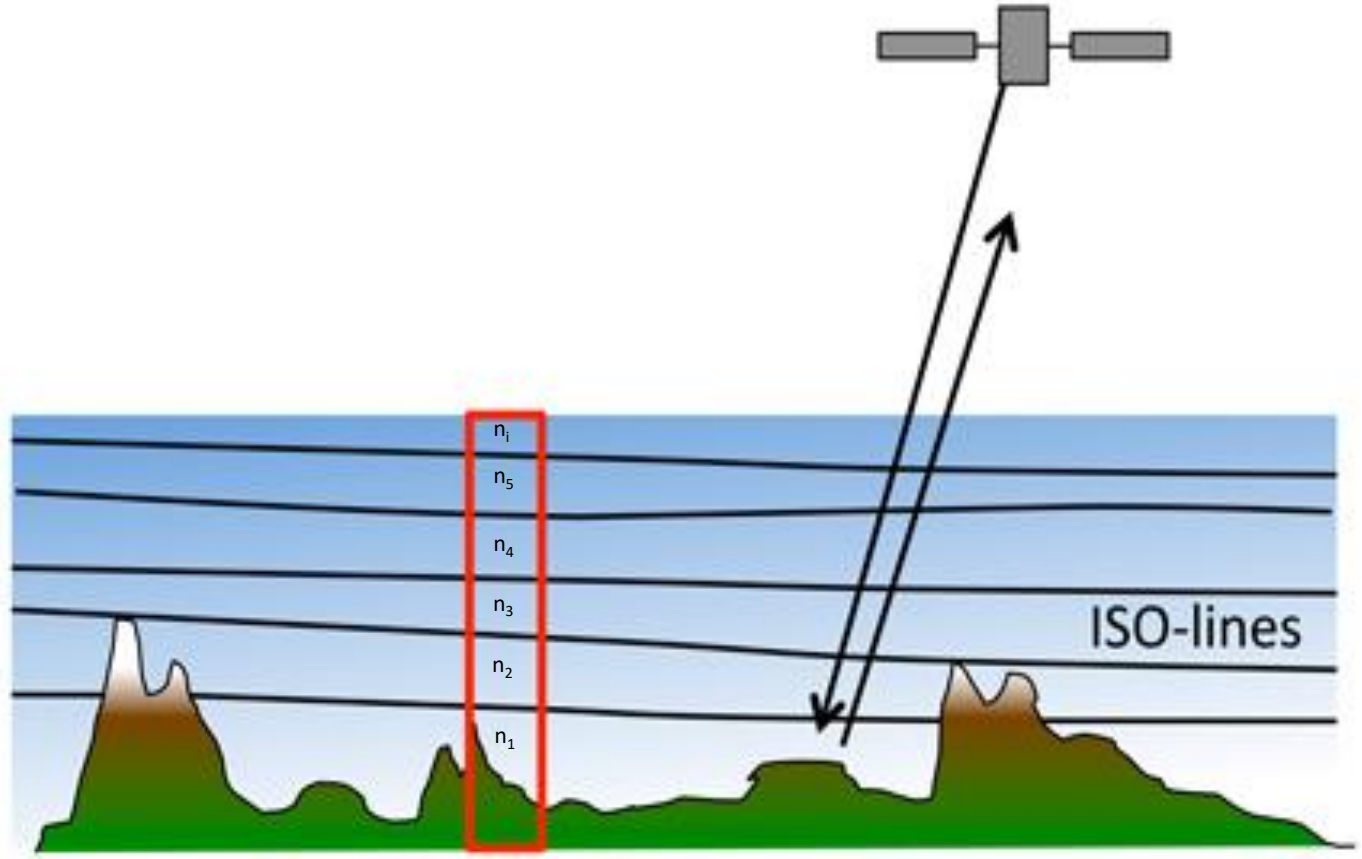

$$\Delta L = \int (n(s) - 1) ds = \int N(s) ds$$

ΔL : Tropospheric path delay

n: tropospheric refractive index
(ratio between the velocity of light and the radiation propagation velocity)

$$\Delta L(zenital) = \int_0^h N(h) dh$$

N : refractivity = $10e^6$ (n-1)

Atmospheric effects

- Weather Research and Forecast (WRF)
- ERA5

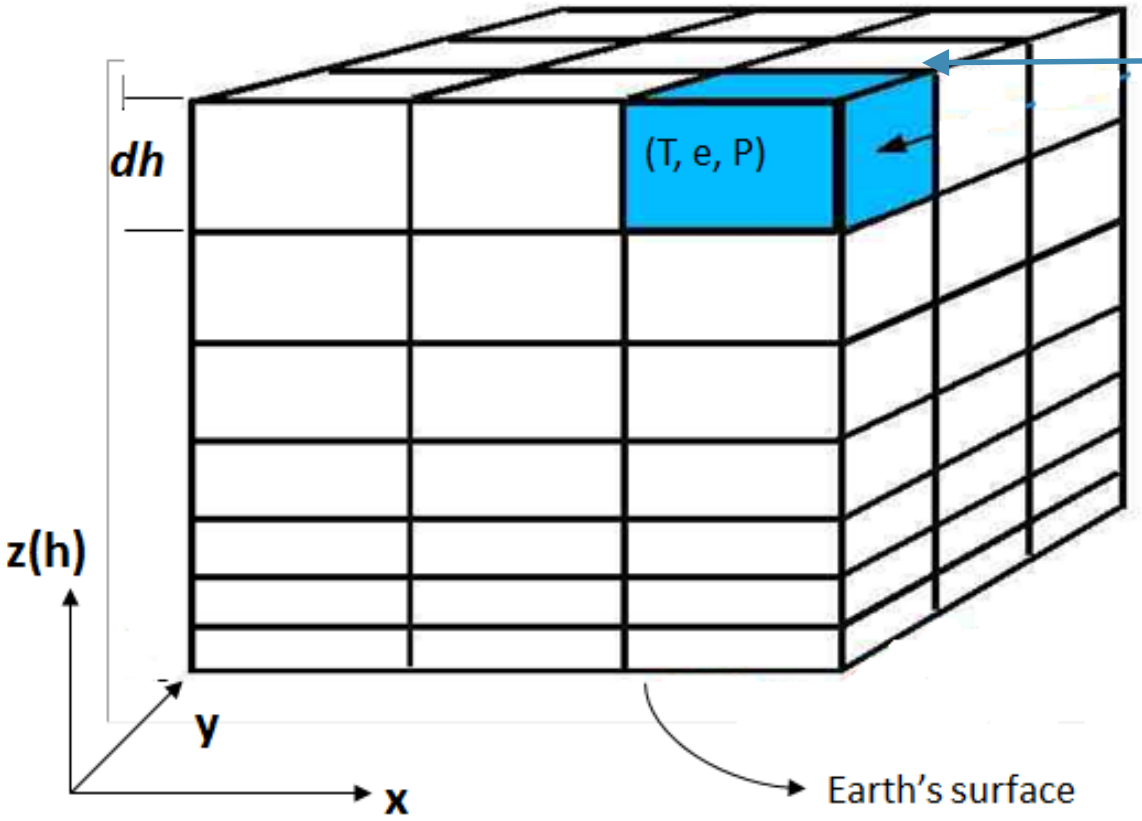

$$T + e + P$$

$$N = \underbrace{k_1 \frac{P}{T}}_{N_{hydrostatic}} + \underbrace{k_2' \frac{e}{T} + k_3 \frac{e}{T^2}}_{N_{wet}}$$

$$\Delta L = ZTD = \sum_{i=1}^{i=L} N_i \cdot dh_i$$

dh: thickness; L: total number of layers

$$DZD = ZTD^{t_m} - ZTD^{t_s}$$

Differential delay between the master and slave images

Mitigating atmospheric effects

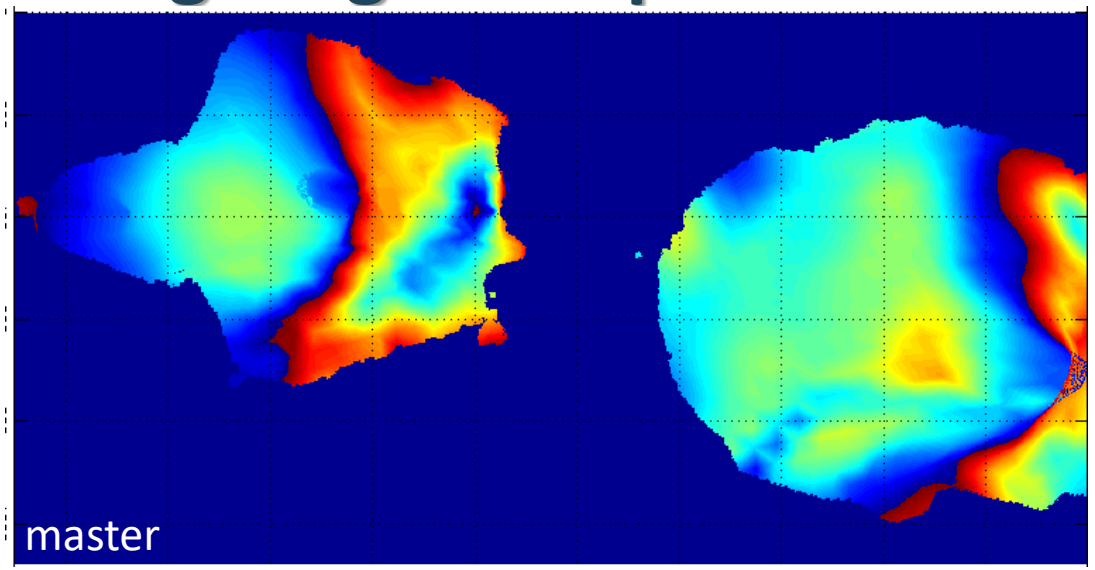

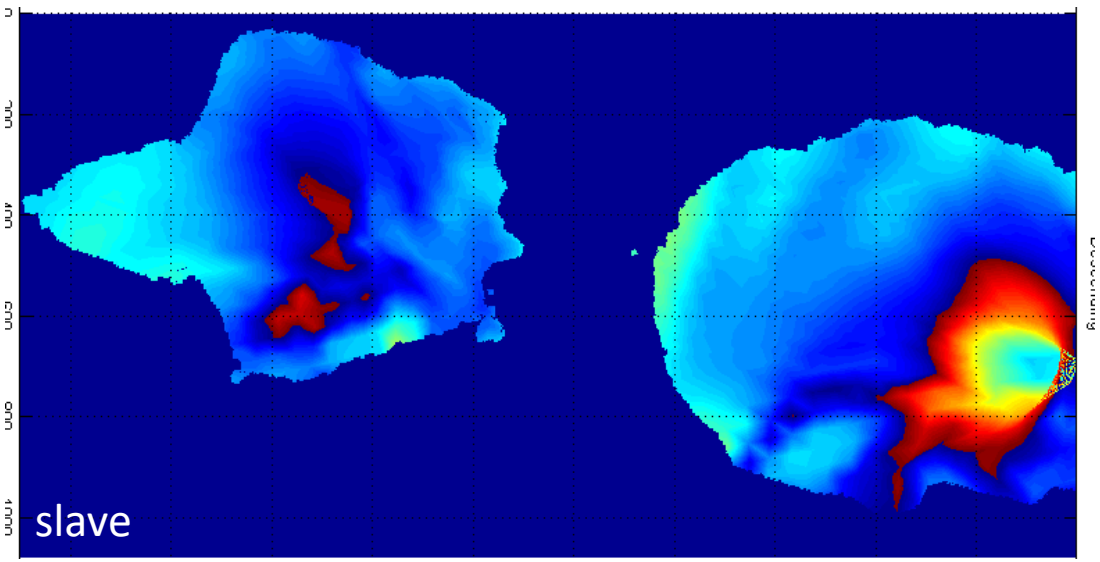

Modelo WRF
Resolução 1km^2

P, e, T

ZTD

SAR + WRF

Amospherally corrected InSAR

PS-InSAR

Processing	PICO	FAIAL
PS	4.6	7.2
PS+WRF	3.7	5.7
PS+GPS	1.9	2.1
PS+WRF+GPS	1.6	1.5

mm/yr

rms of the difference in velocity GPS e PSInSAR

Catalão, et al., 2011.

2015/9/6 18:10

2015/9/7 6:10

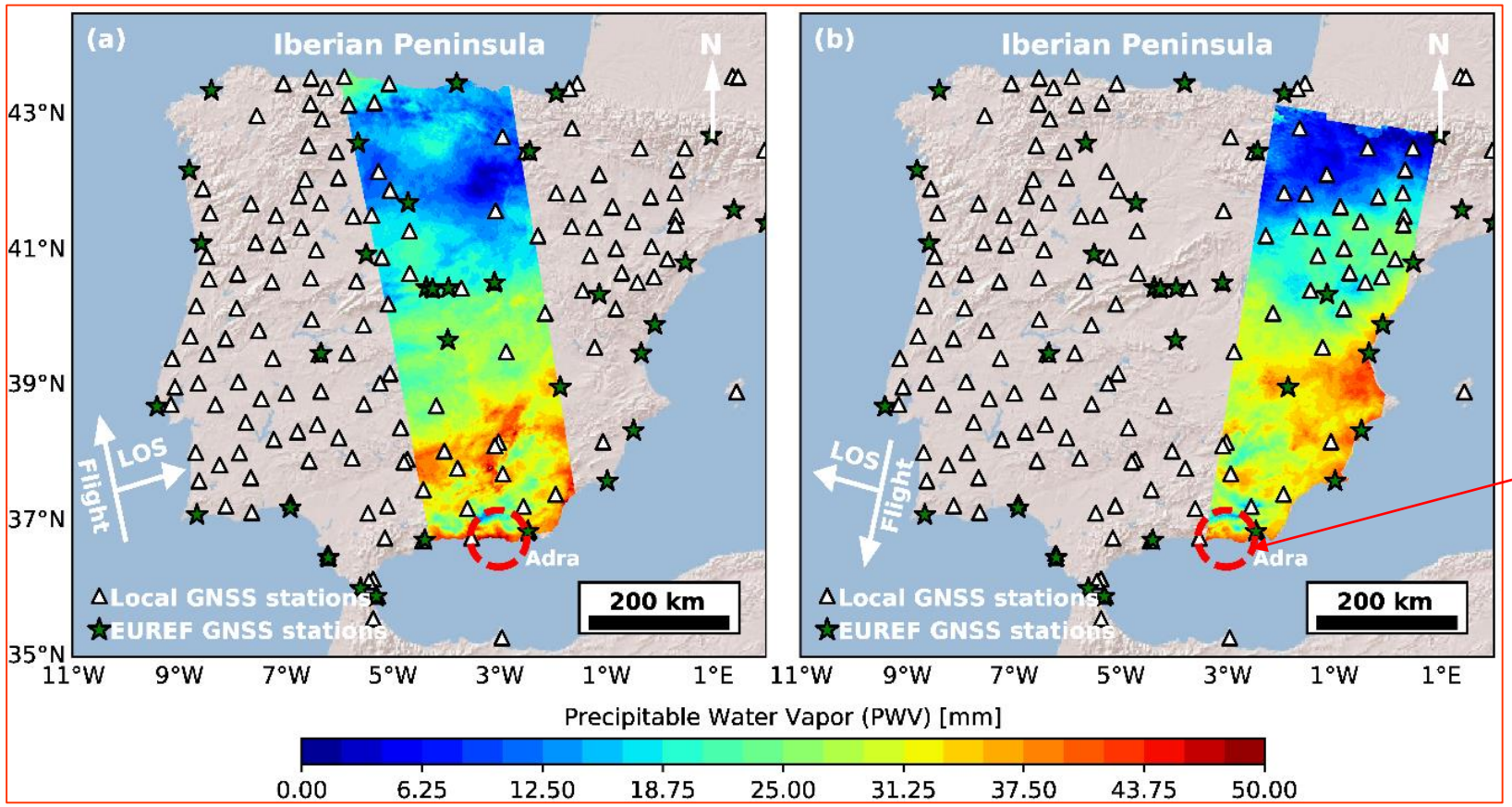

Rain

First storm

Second storm

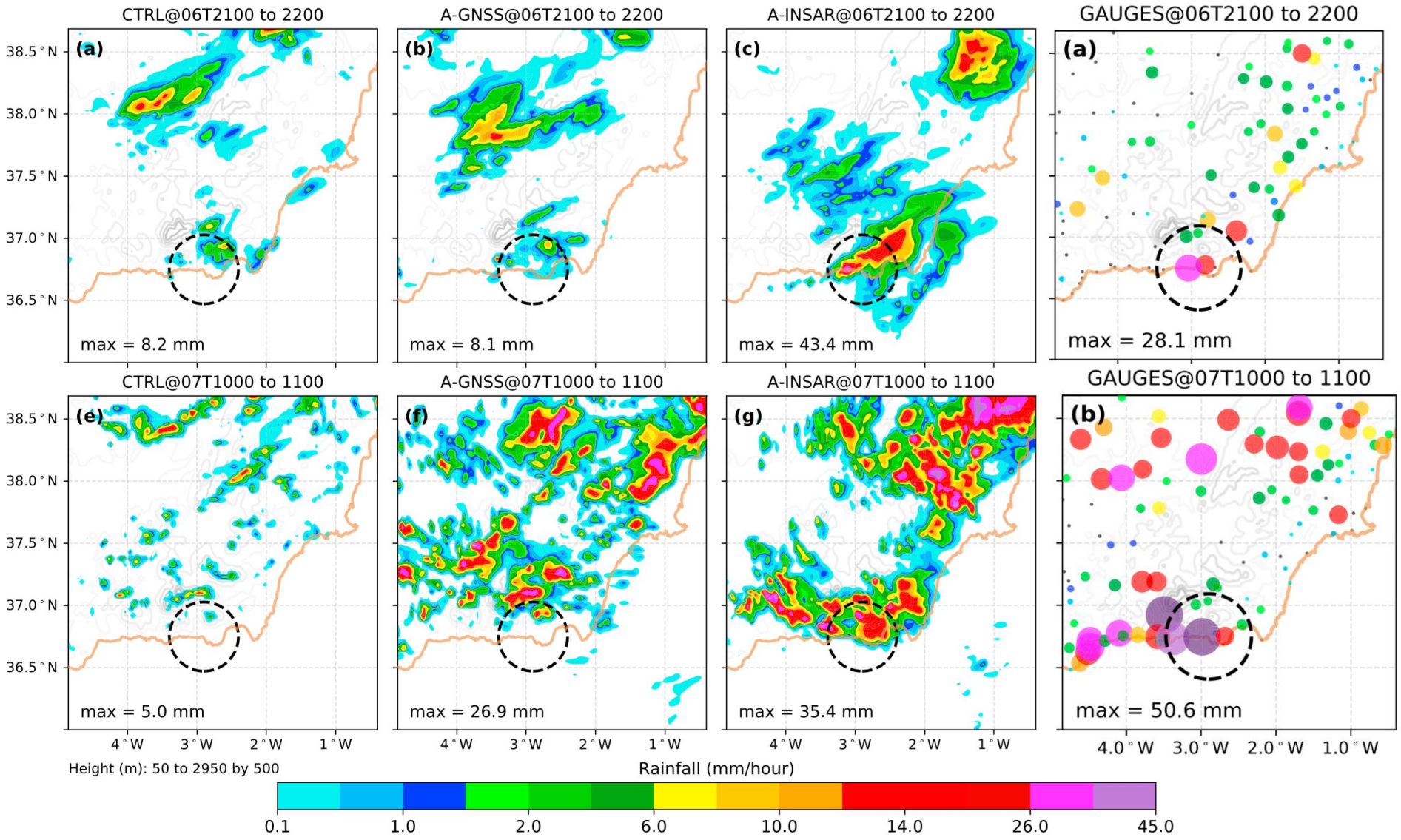

Outlook for synthetic aperture radar

SAR

SAR Polarimetry

InSAR

SAR

InSAR

SAR

InSAR

SAR Polarimetry

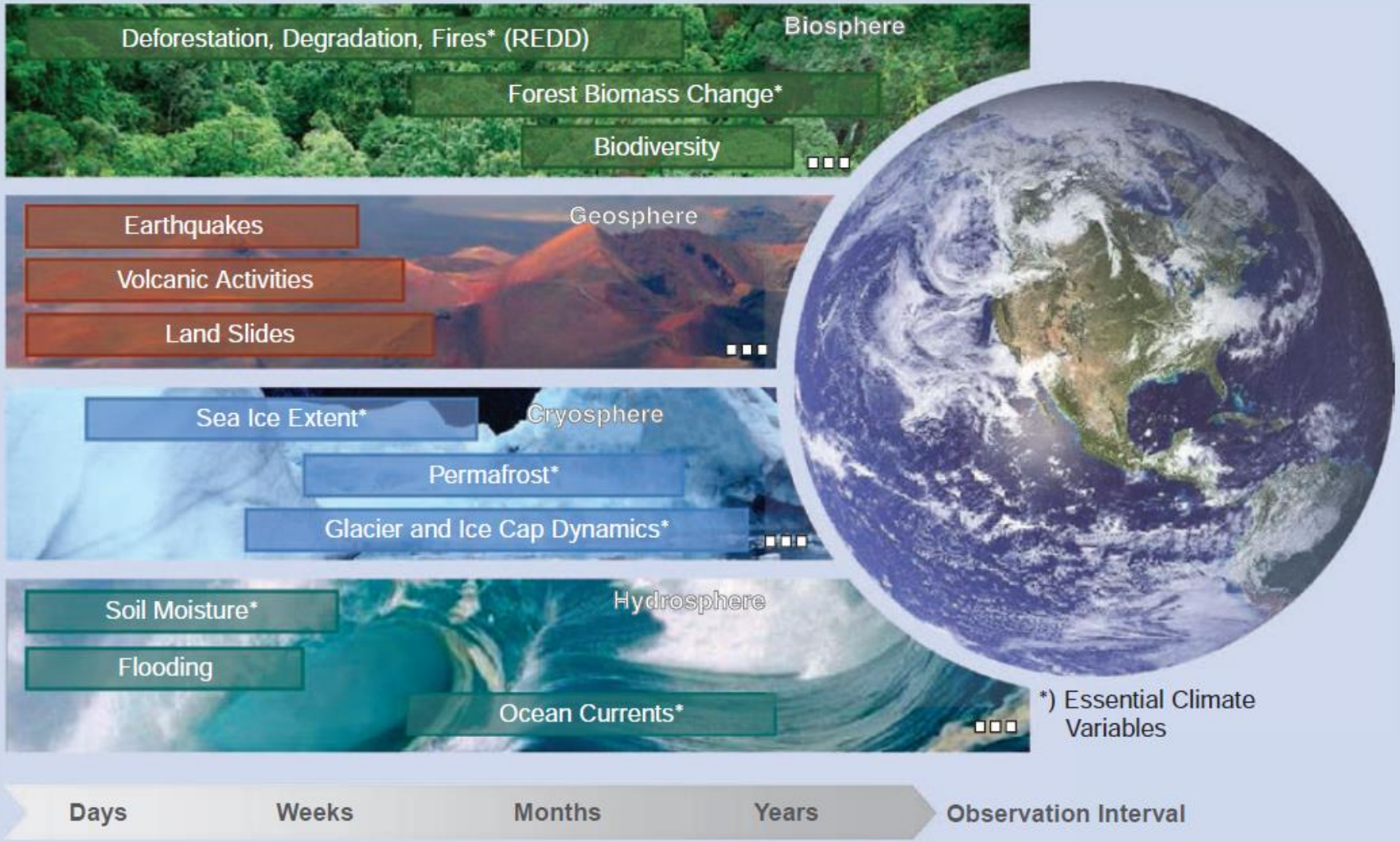

(Moreira et al, 2013)

Síntese

> Differential Synthetic Aperture Radar Interferometry
Potentialities and Limitations

> Persistent Scatterer vs Distributed Scatterer

> Técnica dos Persistent Scatterer,
approach Ferretti et al. e Hooper et al., 2004
Amplitude analysis vs Phase Analysis

> INSAR integration with GPS

> Mitigating atmospheric effects

Improved strain estimation

> ESA / COPERNICUS, Global Monitoring for Environment and Security